SANDIA REPORT
SAND2012-10683
Unlimited Release
Printed April 2013

Comparison of the High Temperature Heat Flux Sensor to Traditional Heat Flux Gages under High Heat Flux Conditions

Thomas K. Blanchat and Charles R. Hanks

Prepared by
Sandia National Laboratories
Albuquerque, New Mexico 87185 and Livermore, California 94550

Sandia National Laboratories is a multi-program laboratory managed and operated by Sandia Corporation, a wholly owned subsidiary of Lockheed Martin Corporation, for the U.S. Department of Energy's National Nuclear Security Administration under contract DE-AC04-94AL85000.

Issued by Sandia National Laboratories, operated for the United States Department of Energy by Sandia Corporation.

Available to DOE and DOE contractors from
U.S. Department of Energy
Office of Scientific and Technical Information
P.O. Box 62
Oak Ridge, TN 37831

Telephone: (865) 576-8401
Facsimile: (865) 576-5728
E-Mail: reports@adonis.osti.gov
Online ordering: http://www.osti.gov/bridge

Available to the public from
U.S. Department of Commerce
National Technical Information Service
5285 Port Royal Rd.
Springfield, VA 22161

Telephone: (800) 553-6847
Facsimile: (703) 605-6900
E-Mail: orders@ntis.fedworld.gov
Online order: http://www.ntis.gov/help/ordermethods.asp?loc=7-4-0#online

SAND2012-10683
Unlimited Release
Printed April 2013

Comparison of the High Temperature Heat Flux Sensor to Traditional Heat Flux Gages under High Heat Flux Conditions

Thomas K. Blanchat and Charles R. Hanks
Fire and Aerosol Sciences
Sandia National Laboratories
P.O. Box 5800
Albuquerque, New Mexico 87185-MSXXXX

Abstract

Four types of heat flux gages (Gardon, Schmidt-Boelter, Directional Flame Temperature, and High Temperature Heat Flux Sensor) were assessed and compared under flux conditions ranging between 100-1000 kW/m^2, such as those seen in hydrocarbon fire or propellant fire conditions. Short duration step and pulse boundary conditions were imposed using a six-panel cylindrical array of high-temperature tungsten lamps. Overall, agreement between all gages was acceptable for the pulse tests and also for the step tests. However, repeated tests with the HTHFS with relatively long durations at temperatures approaching 1000°C showed a substantial decrease (10-25%) in heat flux subsequent to the initial test, likely due to the mounting technique. New HTHFS gages have been ordered to allow additional tests to determine the cause of the flux reduction.

ACKNOWLEDGMENTS

The authors would like to acknowledge the contributions of the following individuals:

- Bennie Belone and Randy Foster (TMSS) for heater array assembly and test unit instrumentation.
- Walt Gill, Jim Nakos, and Jill Suo-Anttila for review, comments and recommendations that clarified and enhanced this report.

CONTENTS

FIGURES

TABLES

NOMENCLATURE

SNL	Sandia National Laboratories
°C	Degrees Celsius
deg	Degree(s)
DFT	Directional Flame Temperature heat flux sensor
Dept.	Department
°F	Degrees Fahrenheit
HTHFS	High Temperature Heat Flux Sensor
MIMS	Mineral-Insulated Metal-Sheathed
OD	Outer Diameter
ref.	Reference
SS	Stainless steel
TC	Thermocouple
TTC	Thermal Test Complex
SCR	Silicon Controlled Rectifier

1. INTRODUCTION

Like many in the thermal test area, Sandia has a need to measure both temperature and heat flux simultaneously in severe environments, such as from liquid hydrocarbon fuel fires or propellant fires. Heat flux is the most challenging of the two desired measurements. In liquid fuel fires, fluxes of up to about 400 kW/m^2 can occur, given an intense enough fire. For propellant fires, 1 MW/m^2 is a common flux level. Commercially available gages (e.g., Gardon and Schmidt-Boelter) work very well in liquid fuel fires, but there are limitations. For propellant fires optical measurements are the most practical method. In either case relatively high uncertainties are common due to several factors (soot build-up, convection, etc.).

There are a number of issues with commercially available gages specific to Sandia tests. Basic configuration of many gages requires a hole in the test surface to mount the gage (~1 inch diameter x 3-4 inches long). Most of our units under test (UUT) cannot accommodate such a hole. There is also a requirement for gage cooling (water cooled gages are the norm for 30-60 minute fires) and providing that cooling can sometimes be difficult. In JP-8 fires soot deposition on the (relatively) cold face causes the gage to foul. Convection in wind-driven fires sometimes is a non-negligible fraction of the total (e.g., 25%). These issues sometimes have resulted in not being able to make heat flux measurements at all in some tests.

Several years ago Sandia contracted with Dr. Tom Diller (Virginia Tech) to try to develop a new gage that had the following characteristics: 1) Flush mount the gage to the unit under test (UUT) without requiring a hole (but could accommodate small holes for screw mounting), 2) No water cooling (or cooling of any kind), 3) Not susceptible to soot deposition, 4) Could withstand temperatures of ~1000°C, and 5) Measure net flux, and infer incident flux using a model (energy balance on gage surface). Dr. Diller and his team developed the "High Temperature Heat Flux Sensor" (HTHFS) which Sandia has been testing for the last several years.

This report compares results of the HTHFS to other gage types using identical short duration high heat flux step and pulse boundary conditions to obtain confidence in gage performance in our applications. The HTHFS was evaluated for robustness. The "hybrid" heat flux data reduction method was used to reduce the HTHFS net heat flux data. Finally, terms were estimated to infer incident heat flux (our applications require boundary conditions for code inputs; this in turn requires incident fluxes rather than net, because net flux is dependent on the surface).

1) A Gardon type heat flux sensor,

2) A Medtherm Schmidt-Boelter type heat flux sensor,

3) A Hukseflux Schmidt-Boelter type heat flux sensor,

4) A Directional Flame Temperature (DFT) heat flux sensor,

5) A Thin Film heat flux sensor (determined to be broken, no results are reported), and

6) A High Temperature Heat Flux Sensor (HTHFS).

2. TEST CONFIGURATION

The set setup consisted of a 6-sided radiant heat array and miscellaneous equipment. An Inconel shroud, typically used in radiant heat tests (the measured shroud temperature provides feedback to control lamp power), was not used in order to achieve the desired step changes in heat flux. Six SCRs (one for each panel) were controlled to provide a profile based on desired percent power. Each water-cooled aluminum lamp panel was almost fully lamped (missing 1 lamp at the bottom, yielding 62 lamps/panel). Assuming each lamp is driven at the rated 6 kW/lamp, each panel requires 372 kW, and a 6-sided array requires ~2.2 MW electrical power. Note that each panel has an average heated area of 0.271 m^2 (420 in^2) and at full power each panel produces a heat flux of ~1372 kW/m^2.

Each gage was tested separately. Figure 1 shows the location of the gage, at the panel bottom and centered in the array (2 panels are swung open for gage installation). All gages were flush mounted, facing upward, centered in an insulated board. The array was open at the top (no top hat or reflector).

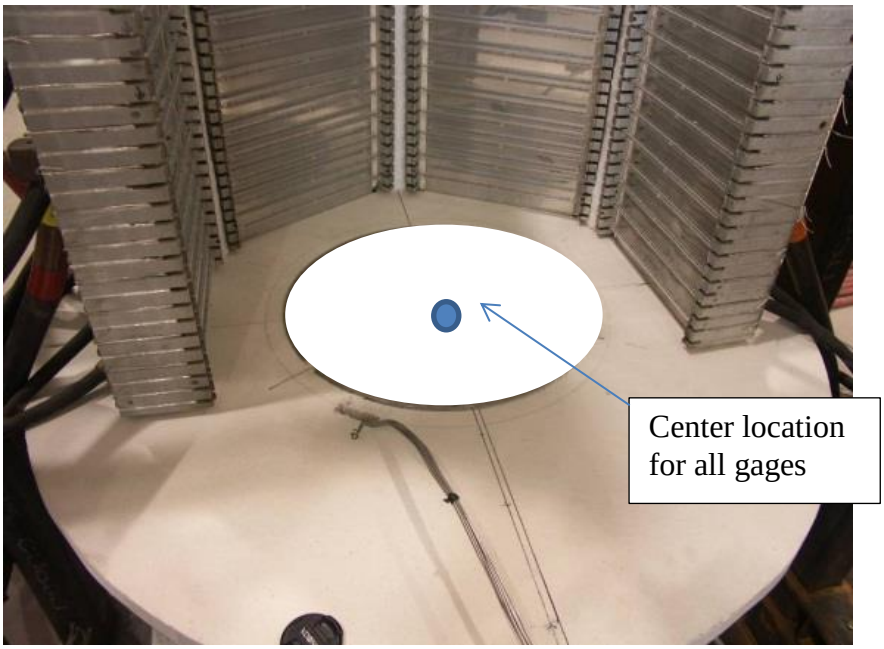

Figure 1 6-Panel Lamp Array

3. HEAT FLUX PROFILES

Each gage was subjected to two profiles, herein called a step profile and a pulse profile, and tested three times at each profile.

The step profile increased SCR power in 10% increments from 0% to 50% and back to 0% with a 20 s duration between steps. Figure 2 shows that the profile was programmed to change the power between steps in 1 s.

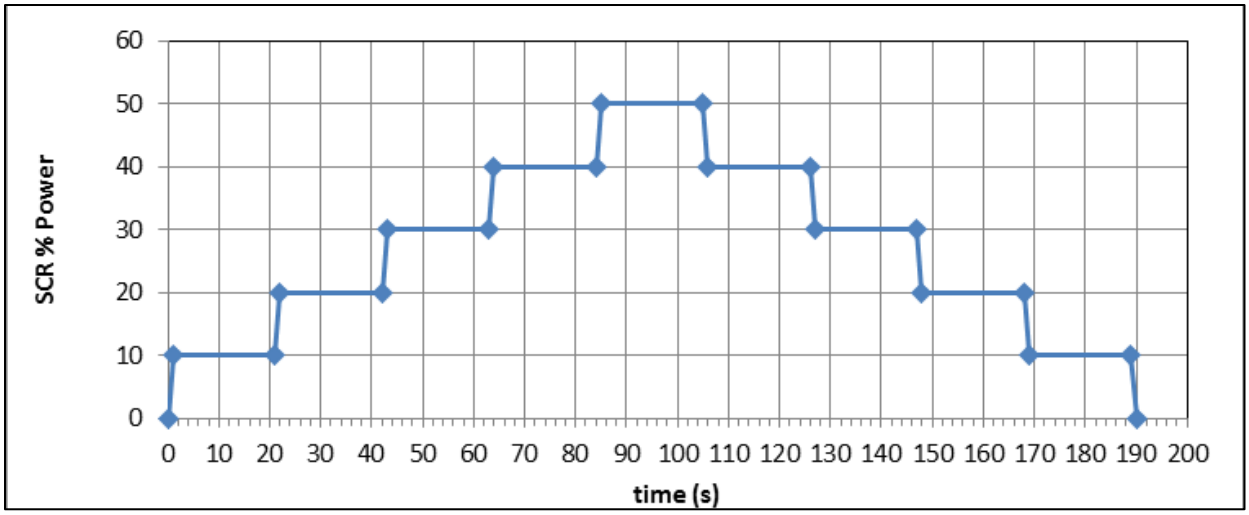

Figure 2 Heat Flux Step Profile

The pulse profile first increased SCR power to 10% power (used to preheat the cold tungsten lamps to prevent thermal shock failure) for 15 s, then increased power to 50% and held for 20 s, then back to 10% power for 15 s (and then off). Figure 3 shows that the profile was programmed to change the power between steps in 1 s. Note that the Hukseflux sensor has an upper heat flux limit of 200 kW/m^2; both the step and the pulse profile peak powers were reduced for that sensor.

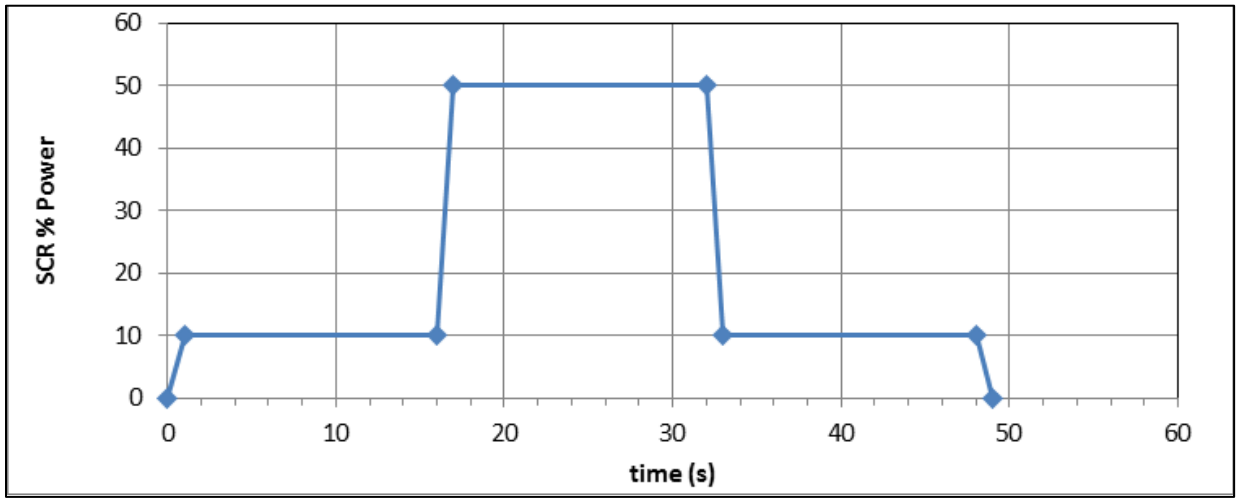

Figure 3 Heat Flux Pulse Profile

4. GARDON TYPE HEAT FLUX SENSOR

The Gardon type heat flux sensor (Figure 4, Medtherm Model 64-100-18 (0-100 BTU/ft^{2}s (0-1.14 MW/m^2), Ser.# 175671, smooth body, no flange, water cooled, 180° view, 0.91 absorptance) measured total heat flux. It had a full scale output of 12.98 mV at 1000 kW/m^2 (yielding an inverse responsivity of 77.04 kW/m^2/mV).

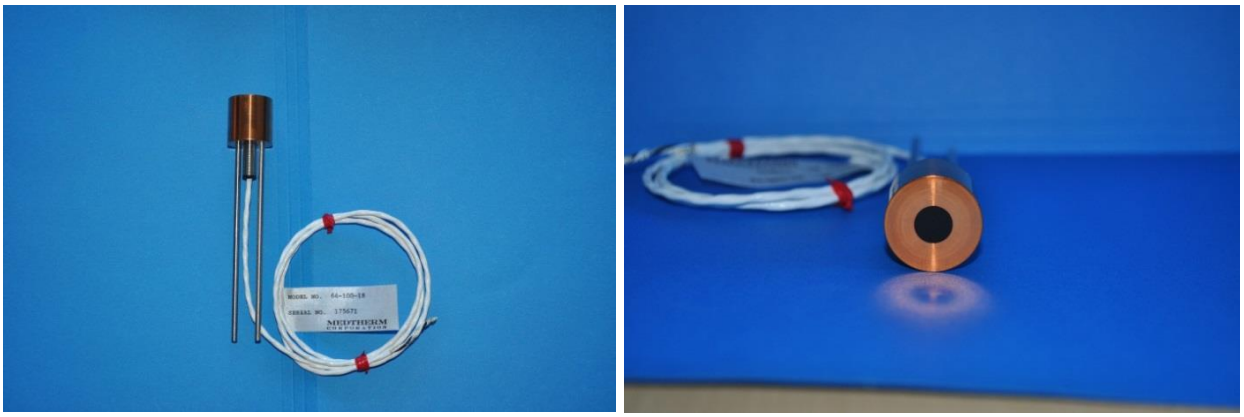

Figure 4 Gardon Total Heat Flux Gage

The Gardon gage, shown in Figure 5, was mounted flush with the insulated board surface, facing upward. A portable chiller was used for cooling water, with the chiller water temperature set to approximately 20°C. Output from the Gardon gage was calibrated to incident heat flux by the manufacturer. Data reduction was based on the manufacturers' calibration data.

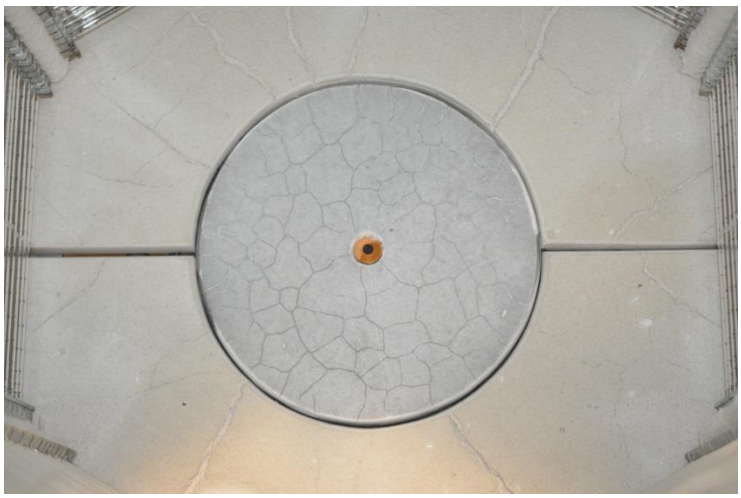

Figure 5 Gardon Gage Mounted inside the 6-Panel Array

In these tests, there was no forced convection, and free convection is minimized by facing the gage upward. However, based on correlations for a flat disc facing upwards, and assuming the gage temperature is 20°C, a convective contribution could be about 10 kW/m^2 at a free stream temperature of 600°C and about 20 kW/m^2 at a free stream temperature of at 1000°C.

Manufacturer's literature for Gardon type gages indicates the accuracy is ~ ±3%. Strictly speaking, this only applies for the calibration which is performed in a radiative only environment. When used in real applications, with small but non-negligible convection, the overall uncertainty can rise significantly. These factors combine to raise the uncertainty of Gardon type gages in fire environments to ~ ±30% (Nakos 2005). Results from the FORUM round robin calibration (Pitts 2004) showed the uncertainties of S-B gages to be ~±8-14%. It will be assumed that the Gardon gage and the Hukseflux gage have similar uncertainties and the larger value from the FORUM report is appropriate in this work.

4.1 Gardon Gage Test Results

4.1.1 Step Test Results

As the Gardon gage results were nearly identical for each of the three step tests, only the detailed data from one step profile are presented. Figure 6 shows the gage heat flux as a function of the SCR power. It also shows the Gardon heat flux gage (HFG) temperature and cooling water return temperature.

The methodology for collecting and comparing the heat flux results for all gages was to visually identify the time at the end of a step or pulse change, subtract one second, and average the previous four seconds of data. These collection times are indicated by the averaging interval shown in Figure 6 and in Table 1.

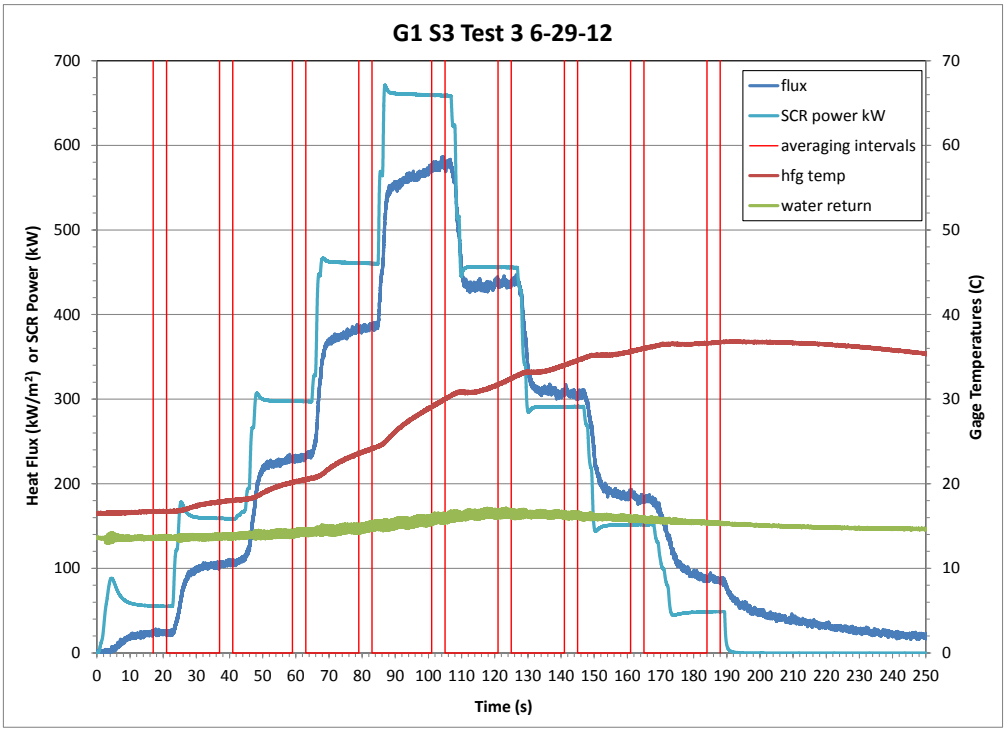

Figure 6 Representative Gardon Gage Step Heat Flux and SCR Power

Figure 7 shows the SCR current and power for the Gardon gage test; the red line at 64 s indicates the end of the 30% step. Figure 8 presents the SCR voltage for the Gardon gage test. SCR power (in kW) was calculated by the summation of the SCR current times the SCR voltage, divided by 1000. Note that the SCRs energized at slightly different times and were small differences between SCR parameters at steady-state (thought to be a function of the hardware and control software).

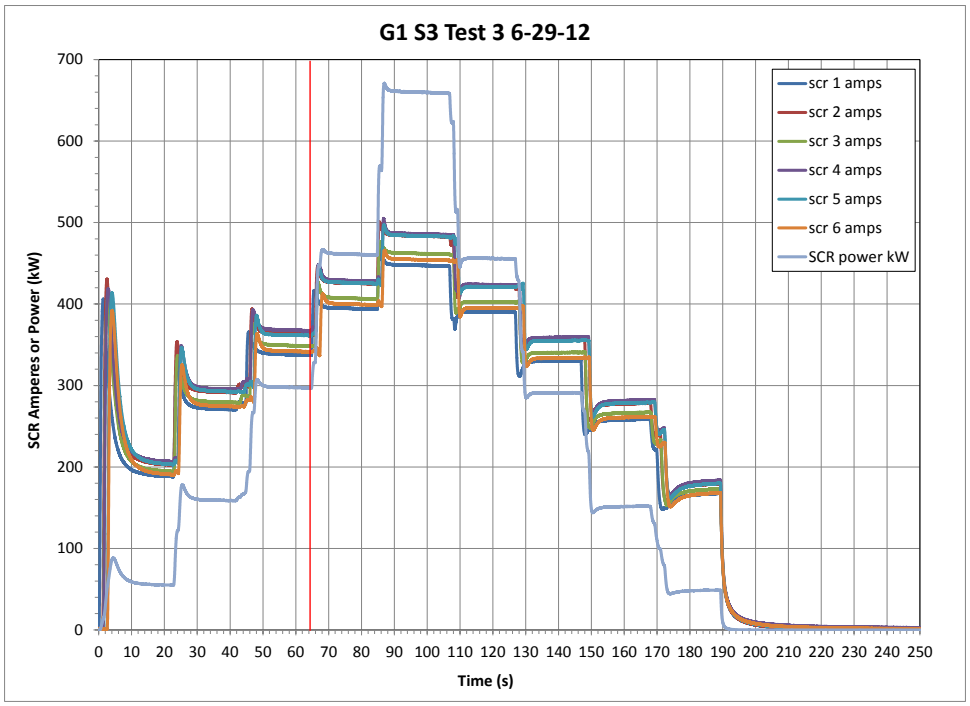

Figure 7 Representative Gardon Gage Step SCR Current and Power

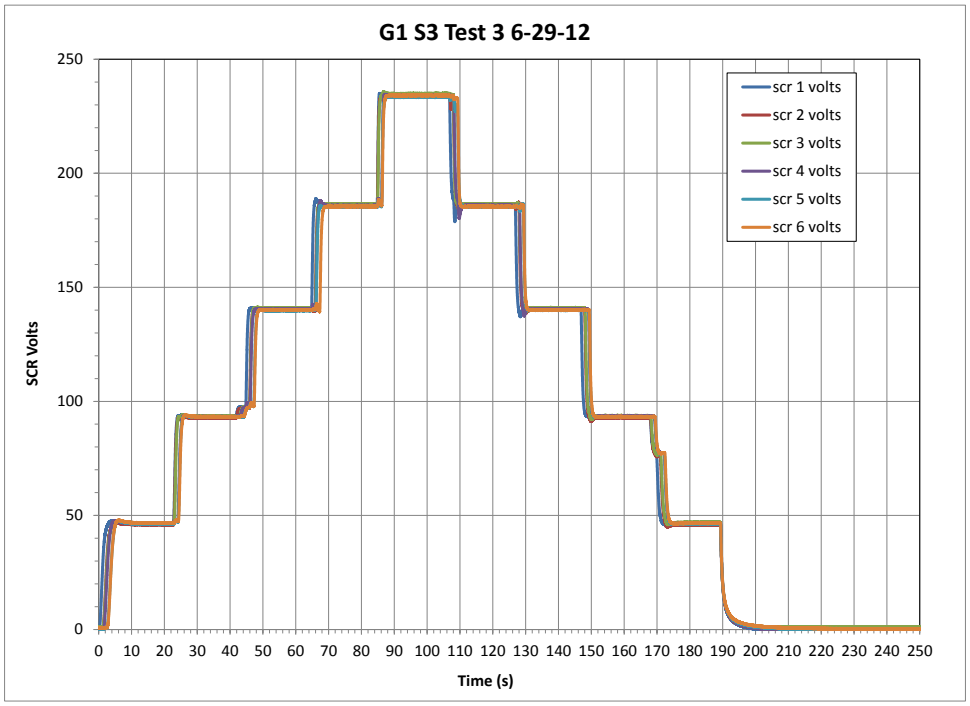

Figure 8 Representative Gardon Gage Step SCR Voltage

Table 1 presents the average and standard deviation (essentially the time variance) of the heat flux and the average SCR power over each of the nine averaging intervals.

Table 1 Gardon Gage Representative Step Test

start s	stop s	end of step s	step	G1 S3 Test 3 6-29-13 SCR %	heat flux average kW/m2	1 std.dev.	SCR power average kW
17	21	22	1	10	24.0	1.2	55.3
37	41	42	2	20	105.7	1.6	158.9
59	63	64	3	30	230.5	1.8	297.5
79	83	84	4	40	383.8	2.1	460.6
101	105	106	5	50	576.1	2.9	659.1
121	125	126	6	40	436.9	2.4	455.8
141	145	146	7	30	306.7	2.8	291.1
161	165	166	8	20	183.7	3.3	151.6
184	188	189	9	10	87.5	2.3	48.7

Table 2 presents the average and one standard deviation of the heat flux (in kW/m^2) and the SCR power (in kW) of the three Gardon gage step tests.

Note that there was essentially no variance in SCR power within the averaging interval during a test. However, individual lamps could (and did) fail during a test; therefore, the average lamp power and standard deviation is reported for each test series (see Table 2 and average results tables for the other gages). The small deviation in SCR power over the three tests was typical for all gages.

Table 2 Gardon Gage Average Results - Three Step Tests

G1 SCR %	G1 Step flux average	1 std.dev.	power average	1 std.dev.
10	22.4	1.5	55.8	0.4
20	103.7	2.0	159.5	0.6
30	228.8	1.6	298.6	1.0
40	381.9	2.7	461.6	1.0
50	572.2	3.4	659.8	1.4
40	435.1	1.6	456.2	0.4
30	305.5	1.2	291.9	0.7
20	182.9	0.8	151.9	0.3
10	87.8	0.5	48.8	0.1

Finally, note that the flux is always greater during the step down portion of SCR power (e.g. 381.9 kW/m^2 at 40% increasing vs. 435.1 kW/m^2 at 40% decreasing). This is attributed to the heating of insulation board, increasing convective flux to gage. This effect is more prevalent in the step tests as compared to the pulse tests due the longer time that the lamps are energized. Note also that water-cooled gages should read higher than uncooled gages due to the convective contribution.

4.1.1 Pulse Test Results

As the Gardon gage results were nearly identical for each of the three pulse tests, only the detailed data from one pulse profile are presented. Figure 9 shows the gage heat flux as a function of the SCR power. It also shows the gage and cooling water return temperature.

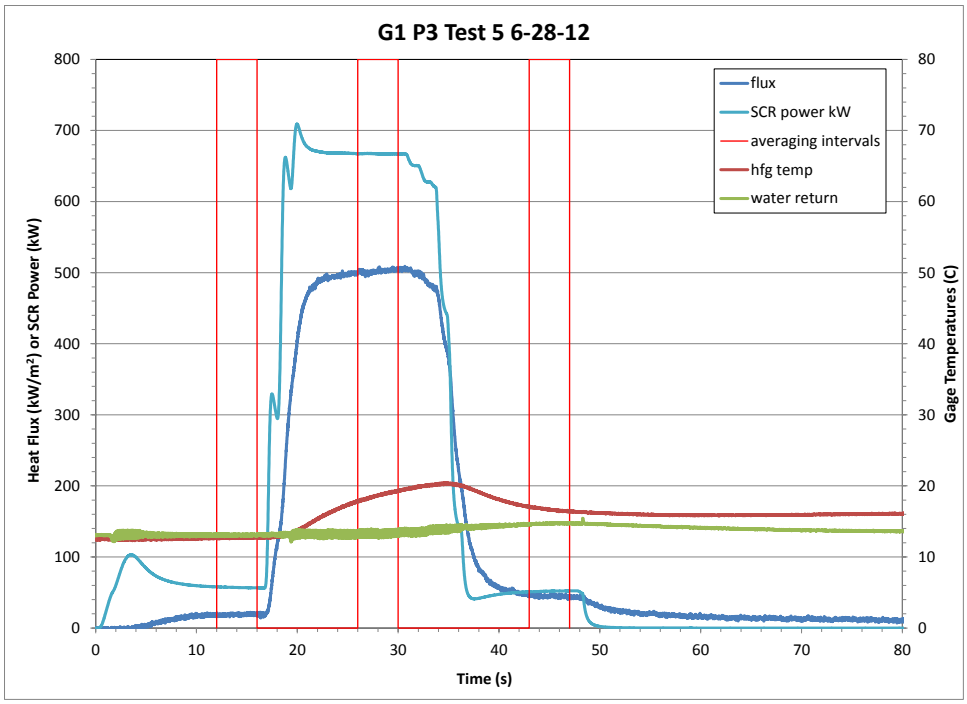

Figure 9 Representative Gardon Gage Pulse Heat Flux and SCR Power

Figure 10 shows the SCR current and power for the Gardon gage test; the red line at 31 s indicates the end of the 50% step. Figure 11 presents the SCR voltage for the Gardon gage test.

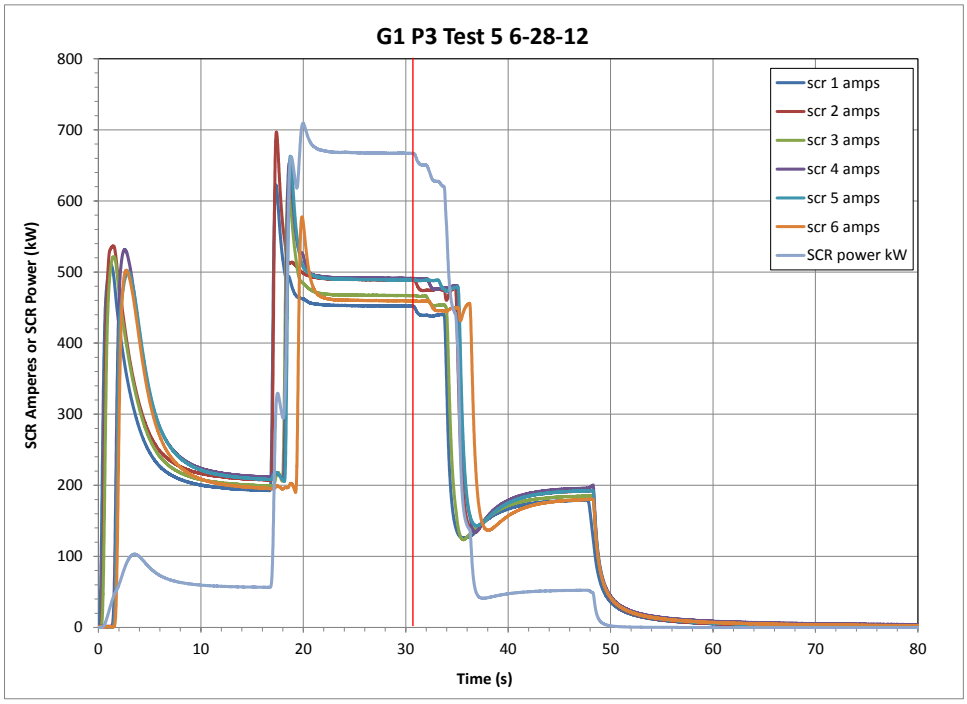

Figure 10 Representative Gardon Gage Pulse SCR Current and Power

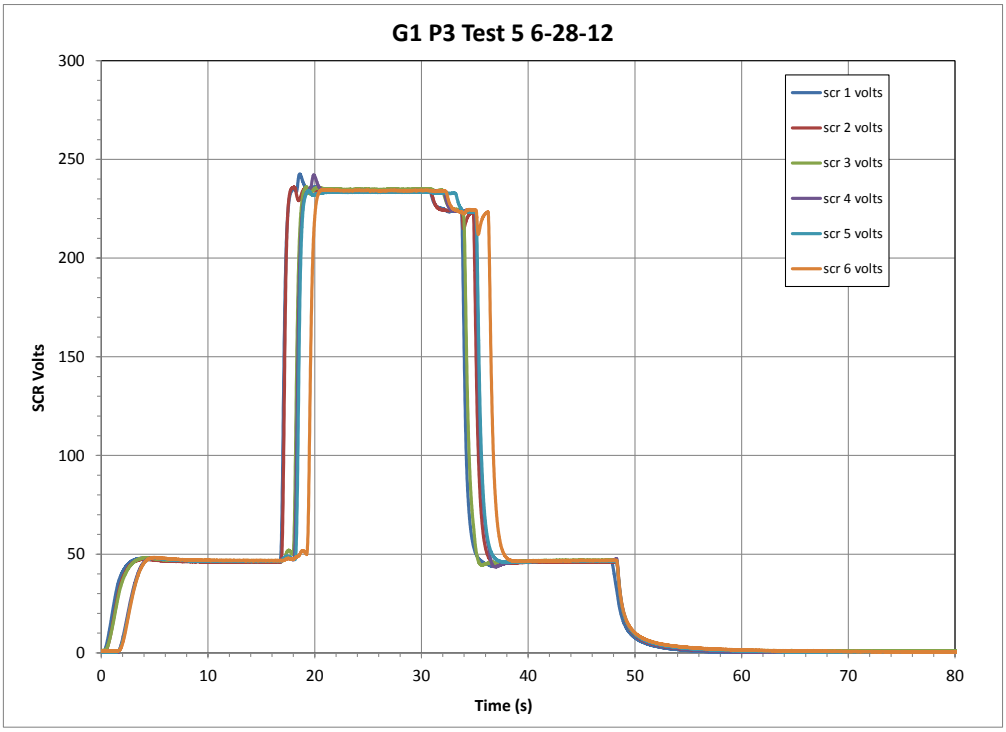

Figure 11 Representative Gardon Gage Pulse SCR Voltage

Table 3 presents the heat flux and SCR power over each of the three averaging intervals.

Table 3 Gardon Gage Representative Pulse Test

start s	stop s	end of step s	step	G1 P3 Test 5 6-28-12 SCR %	heat flux average kW/m2	1 std.dev.	SCR power average kW
12	16	17	1	10	19.0	1.2	57.1
26	30	31	2	50	502.1	2.1	667.3
43	47	48	3	10	45.0	1.5	51.8

Table 4 presents the average and standard deviation of the heat flux (in kW/m^2) and the SCR power (in kW) of the three Gardon gage pulse tests.

Table 4 Gardon Gage Average Results - Three Pulse Tests

G1 SCR %	G1 Pulse flux average	1 std.dev.	power average	1 std.dev.
10	19.1	0.3	57.4	0.2
50	502.6	1.1	668.7	1.5
10	45.0	0.4	51.9	0.2

5. SCHMIDT-BOELTER TYPE HEAT FLUX SENSOR

A Schmidt-Boelter type heat flux sensor, (Figure 12, Medtherm Model 64-100SB-18 (0-100 BTU/ft^{2}s (0-1.14 MW/m^2), Ser. # 175701, smooth body, no flange, water cooled, 180° view, 0.90 absorptance) measured total heat flux. It had a full scale output of 25.29 mV at 1000 kW/m^2 (yielding an inverse responsivity of 39.54 kW/m^2/mV).

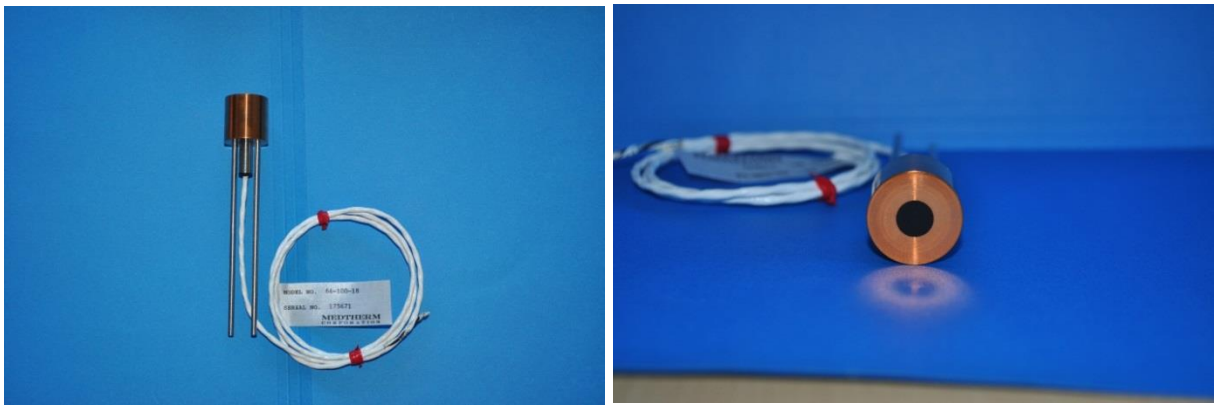

Figure 12 Schmidt-Boelter Type Heat Flux Sensor

The Schmidt-Boelter gage, shown in Figure 13, was mounted flush with the insulated board surface, facing upward. A portable chiller was used for cooling water, with the chiller water temperature set to approximately 20°C. Output from the Schmidt gage was calibrated to absorbed heat flux by the manufacturer; the flux results were divided by the absorptance (0.90) to convert to incident heat flux.

Data reduction was based on the manufacturers' calibration data.

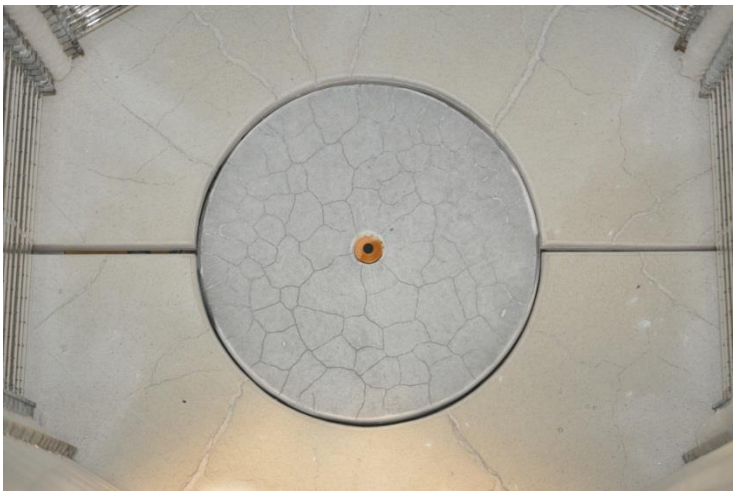

Figure 13 Schmidt-Boelter Mounted inside the 6-Panel Array

5.1 Schmidt-Boelter Gage Test Results

5.1.1 Step Test Results

As the Schmidt-Boelter gage results were nearly identical for each of the three step tests, only the detailed data from one step profile are presented. Figure 14 shows the gage heat flux as a function of the SCR power. It also shows the gage and cooling water return temperature.

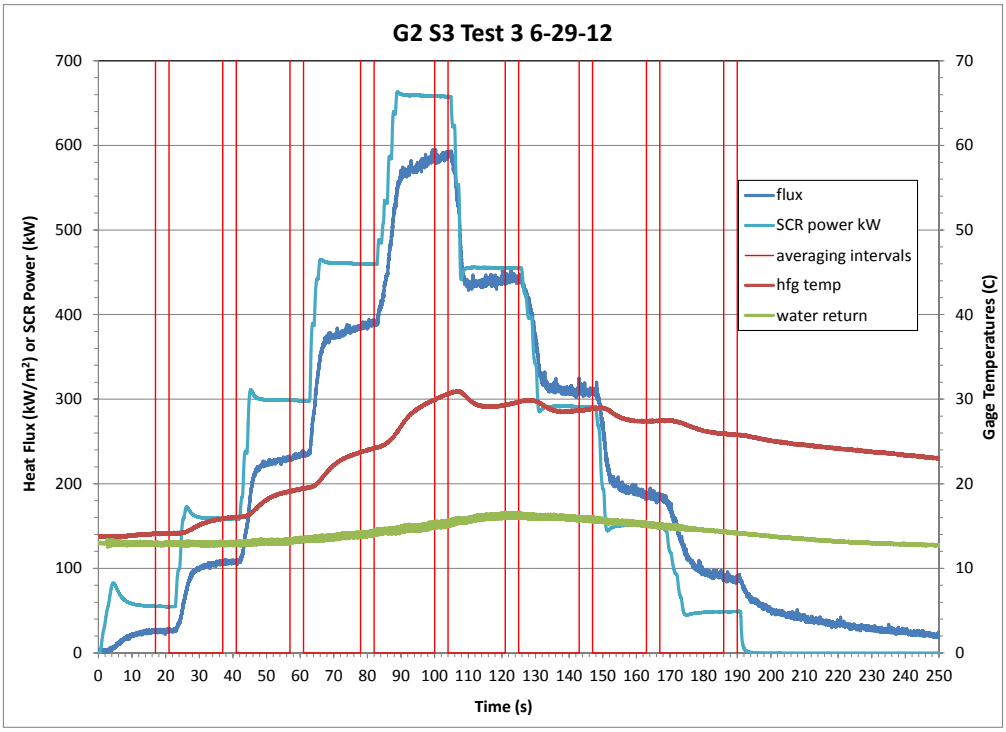

Figure 14 Representative Schmidt-Boelter Gage Step Heat Flux and SCR Power

Figure 15 shows the SCR current and power for the Schmidt-Boelter gage test; the red line at 63 s indicates the end of the 30% step. Figure 16 presents the SCR voltage for the Schmidt-Boelter gage test.

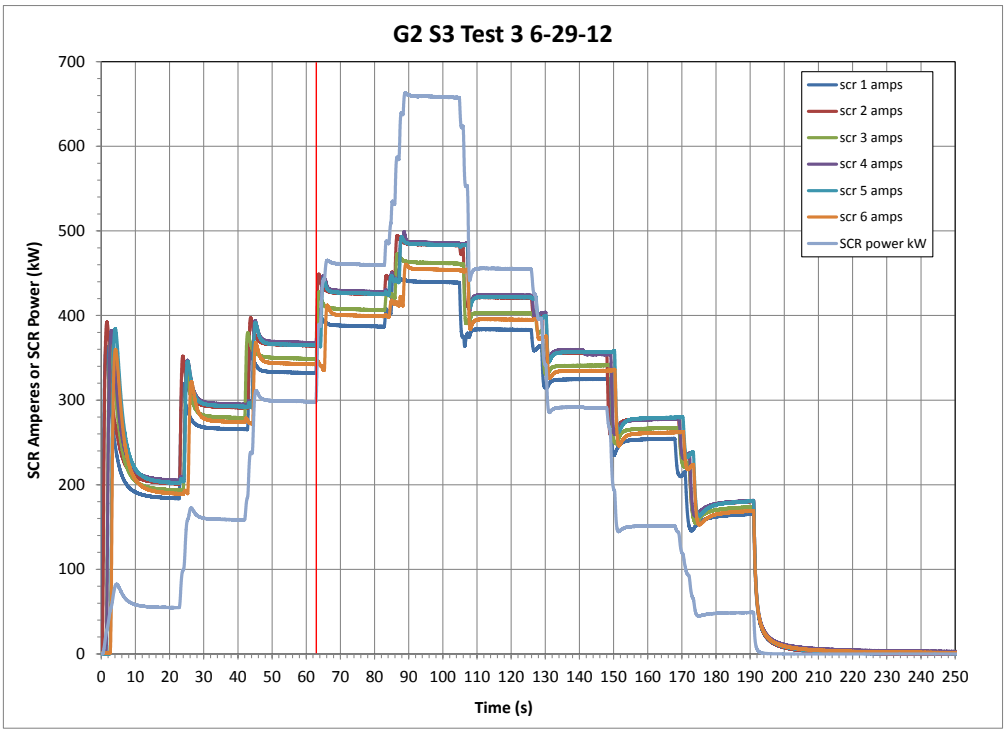

Figure 15 Representative Schmidt-Boelter Gage Step SCR Current and Power

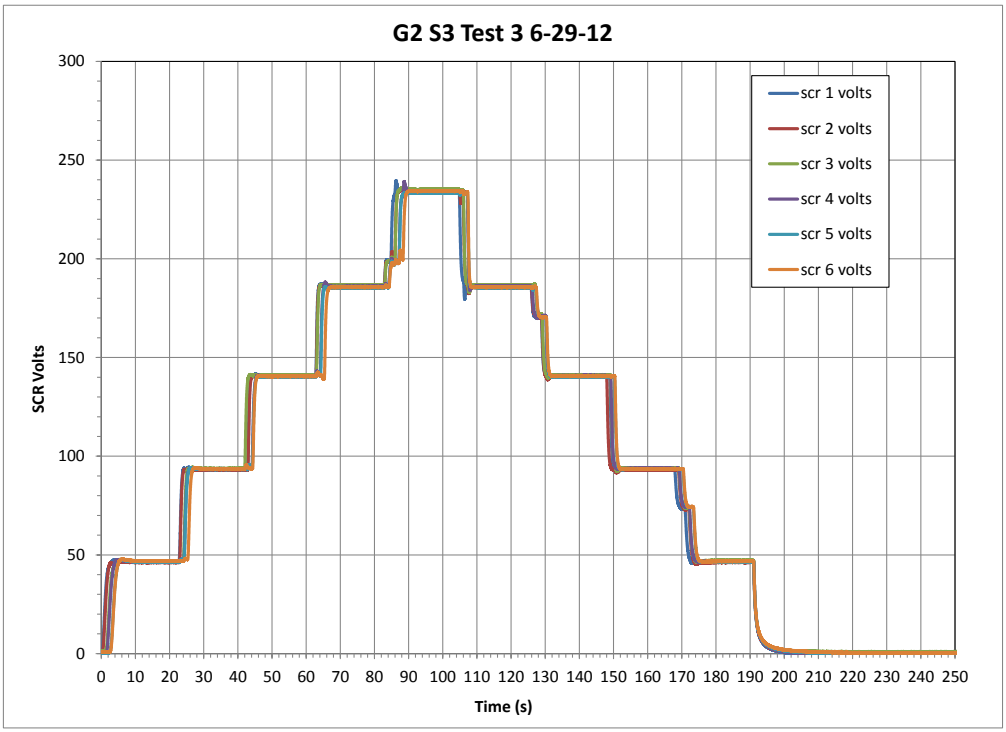

Figure 16 Representative Schmidt-Boelter Gage Step SCR Voltage

Table 5 presents the heat flux and SCR power over each of the nine averaging intervals.

Table 5 Schmidt-Boelter Gage Representative Step Test

start s	stop s	end of step s	step	G2 S3 Test 3 6-29-12 SCR %	heat flux average kW/m2	1 std.dev.	SCR power average kW
17	21	22	1	10	26.1	0.9	55.0
37	41	42	2	20	107.3	1.0	158.8
57	61	62	3	30	232.5	2.0	298.4
78	82	83	4	40	388.1	2.4	459.8
100	104	105	5	50	586.2	3.2	658.0
121	125	126	6	40	442.2	2.8	455.1
143	147	148	7	30	309.0	2.6	291.0
163	167	168	8	20	185.0	2.4	151.5
186	190	191	9	10	87.6	2.1	48.8

Table 6 presents the average and standard deviation of the heat flux (in kW/m^2) and the SCR power (in kW) of the three Schmidt-Boelter gage step tests.

Table 6 Schmidt-Boelter Gage Average Results - Three Step Tests

G2 SCR %	G2 Step flux average	1 std.dev.	power average	1 std.dev.
10	26.1	0.9	55.7	0.9
20	107.3	1.0	159.7	1.4
30	232.5	2.0	299.5	2.5
40	388.1	2.4	461.5	2.9
50	586.2	3.2	659.8	3.4
40	442.2	2.8	456.0	1.6
30	309.0	2.6	292.0	1.5
20	185.0	2.4	152.0	0.9
10	87.6	2.1	48.9	0.4

5.1.2 Pulse Test Results

As the Schmidt-Boelter gage results were nearly identical for each of the three pulse tests, only the detailed data from one pulse profile are presented. Figure 17 shows the gage heat flux as a function of the SCR power. It also shows the gage and cooling water return temperature.

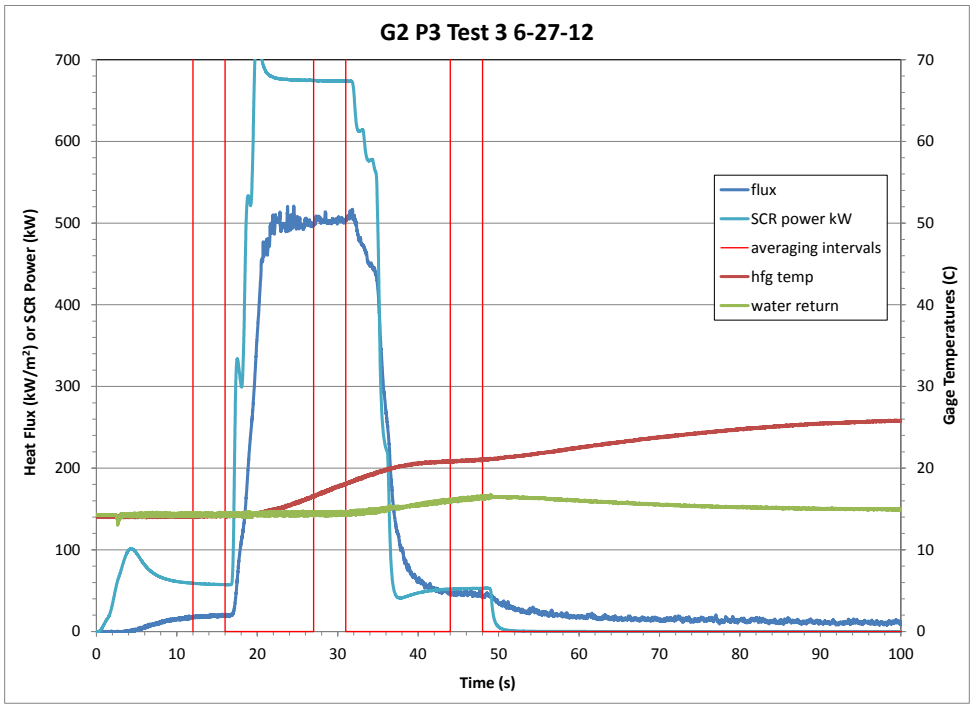

Figure 17 Representative Schmidt-Boelter Pulse Heat Flux and SCR Power

Figure 18 shows the SCR current and power for the Schmidt-Boelter gage test; the red line at 17 s indicates the end of the 10% step. Figure 19 presents the SCR voltage for the Schmidt-Boelter gage test.

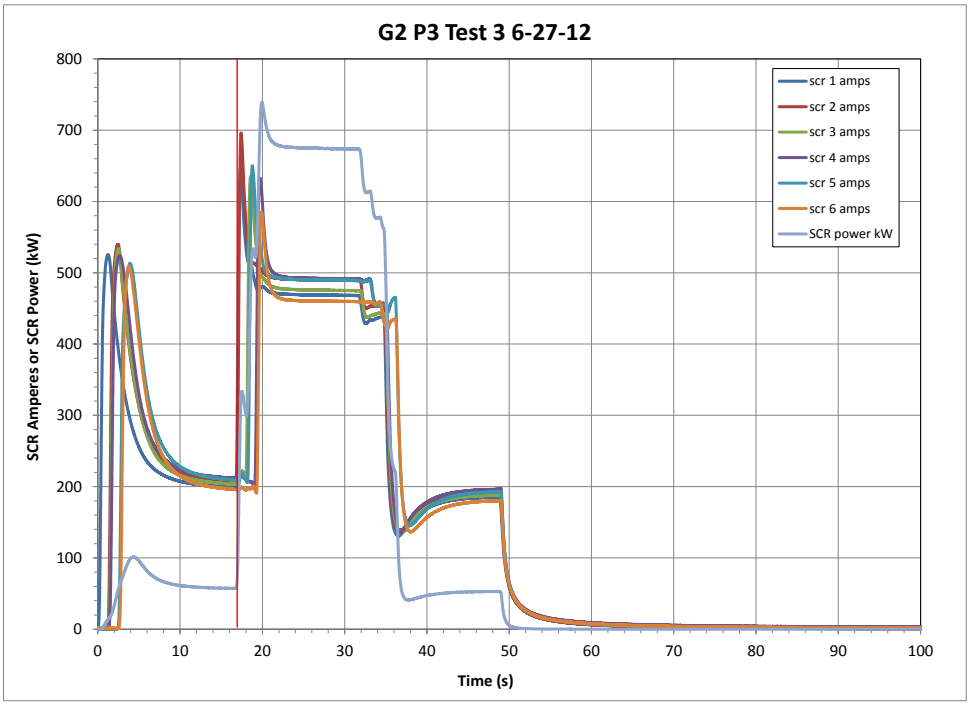

Figure 18 Representative Schmidt-Boelter Pulse SCR Current and Power

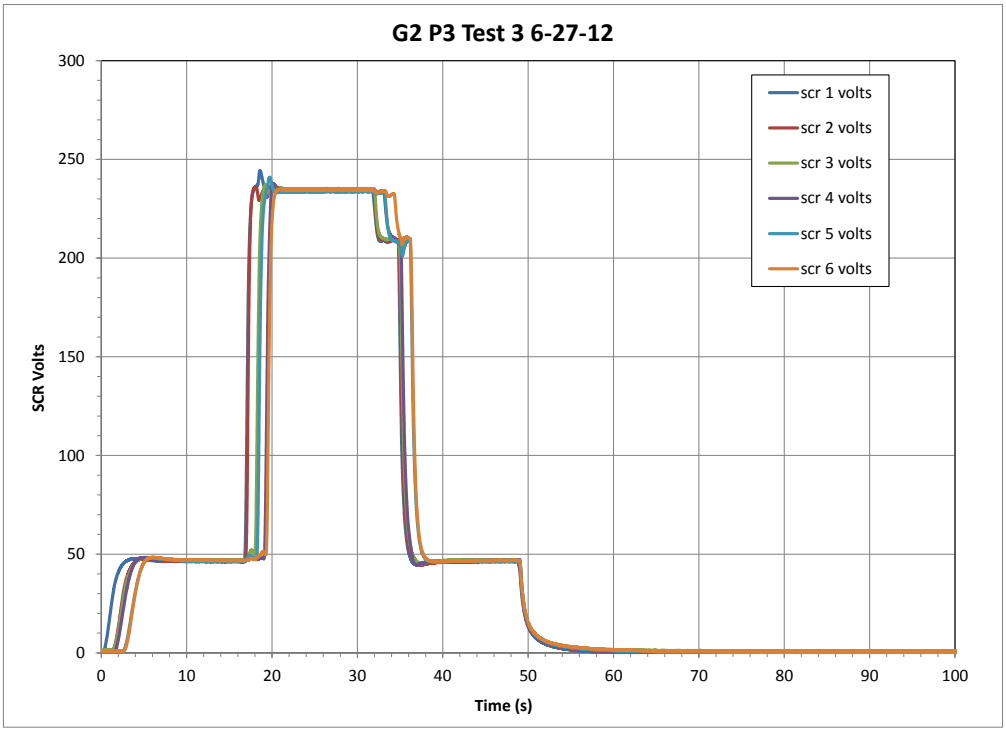

Figure 19 Representative Schmidt-Boelter Pulse SCR Voltage

Table 7 presents the heat flux and SCR power over each of the three averaging intervals.

Table 7 Schmidt-Boelter Representative Pulse Test

start s	stop s	end of step s	step	G2 P3 Test 3 6-27-12 SCR %	heat flux average kW/m2	1 std.dev.	SCR power average kW
12	16	17	1	10	18.8	0.9	58.0
27	31	32	2	50	503.1	2.8	674.1
44	48	49	3	10	46.2	1.5	52.5

Table 8 presents the average and standard deviation of the heat flux (in kW/m^2) and the SCR power (in kW) of the three Schmidt-Boelter gage pulse tests.

Table 8 Schmidt-Boelter Gage Average Results - Three Pulse Tests

G2 SCR %	G2 Pulse flux average	1 std.dev.	power average	1 std.dev.
10	19.0	0.3	57.5	0.5
50	506.1	2.8	669.6	3.9
10	45.4	0.7	52.0	0.4

6. HUKSEFLUX HEAT FLUX SENSOR

A Schmidt-Boelter type heat flux sensor, the Hukseflux Model SBG01-200 (Figure 20, 0-200 kW/m^2 (0-17.5 BTU/ft^{2}s), Ser. #1051, smooth body, with flange, water cooled, ~180° view, >0.95 emissivity) measured total heat flux. It had a full scale output of 31.4 mV at 200 kW/m^2 (yielding an inverse responsivity of 6.369 kW/m^2/mV).

Figure 20 Hukseflux Total Heat Flux Gage

The Hukseflux gage, shown in Figure 21, was mounted flush with the insulated board surface, facing upward. A portable chiller was used for cooling water, with the chiller water temperature set to approximately 20°C. Output from the Hukseflux gage was calibrated to incident heat flux by the manufacturer. Data reduction was based on the manufacturers' calibration data.

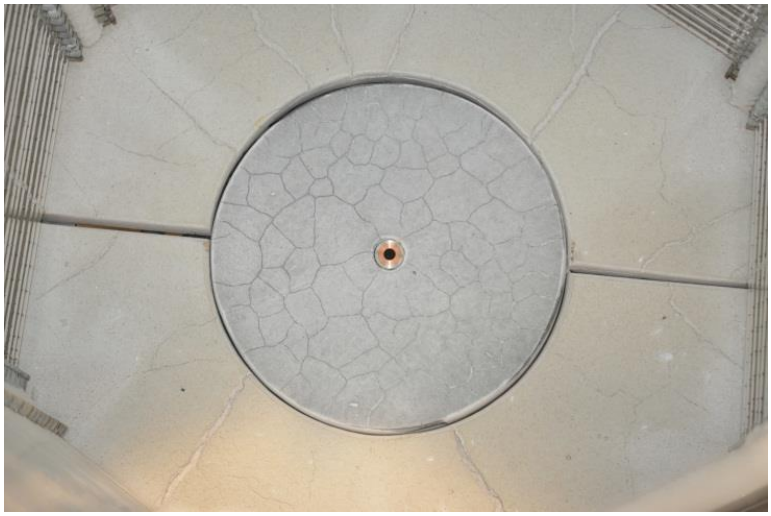

Figure 21 Hukseflux Mounted inside the 6-Panel Array

6.1 Hukseflux Test Results

6.1.1 Step Test Results

As the Hukseflux gage results were nearly identical for each of the three step tests, only the detailed data from one step profile are presented. Figure 22 shows the gage heat flux as a function of the SCR power. It also shows the gage and cooling water return temperature. Note that due to the maximum range of 200 kW/m2, the maximum step of the SCRs was 30% power.

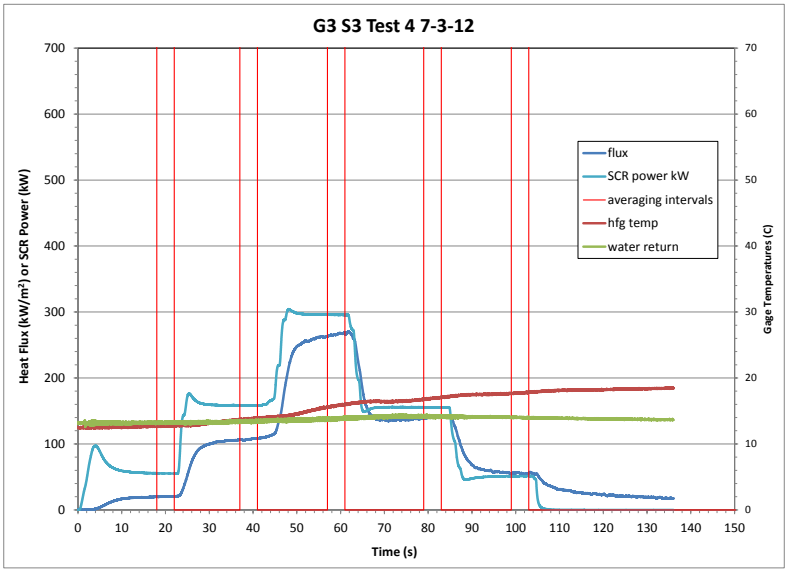

Figure 22 Representative Hukseflux Gage Step Heat Flux and SCR Power

Figure 23 shows the SCR current and power for the Hukseflux gage test; the red line at 23 s indicates the end of the 10% step. Figure 24 presents the SCR voltage for the Hukseflux gage test.

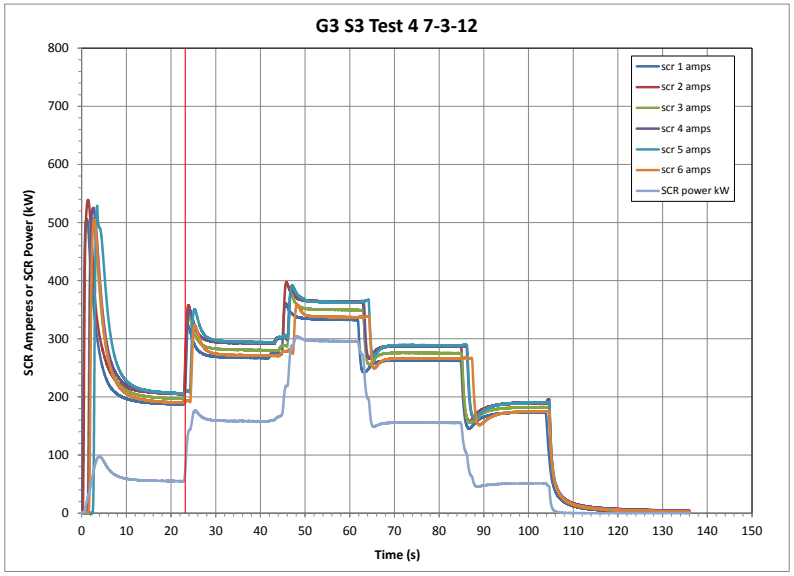

Figure 23 Representative Hukseflux Gage Step SCR Current and Power

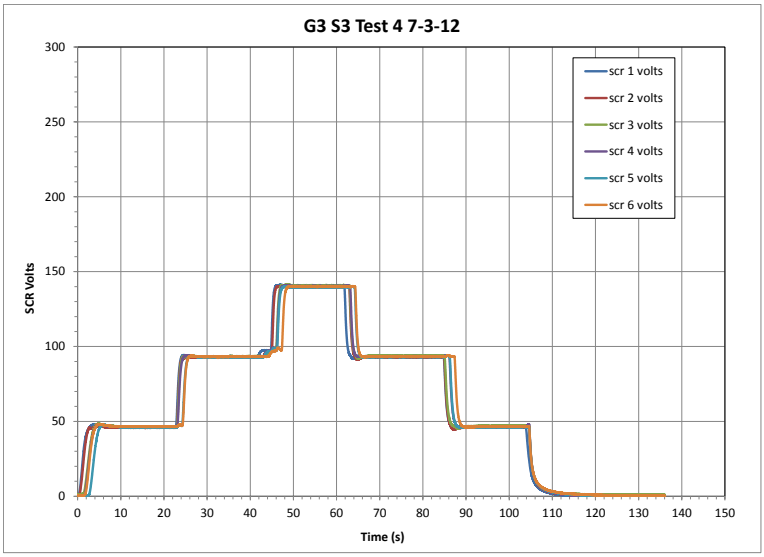

Figure 24 Representative Hukseflux Gage Step SCR Voltage

Table 9 presents the heat flux and SCR power over each of the five averaging intervals.

Table 9 Hukseflux Gage Representative Step Test

start s	stop s	end of step s	step	G3 S3 Test 4 7-3-12 SCR %	heat flux average kW/m2	1 std.dev.	SCR power average kW
18	22	23	1	10	20.2	0.2	55.3
37	41	42	2	20	107.1	0.9	158.2
57	61	62	3	30	266.1	1.5	295.8
79	83	84	4	20	140.3	0.9	155.5
99	103	104	5	10	55.4	0.9	51.1

Table 10 presents the average and standard deviation of the heat flux (in kW/m^2) and the SCR power (in kW) of the three Hukseflux gage step tests.

Table 10 Hukseflux Gage Average Results - Three Step Tests

G3 SCR %	G3 Step flux average	1 std.dev.	power average	1 std.dev.
10	26.1	0.9	55.4	0.1
20	107.3	1.0	158.3	0.1
30	232.5	2.0	295.8	0.3
40	388.1	2.4	155.3	0.2
50	586.2	3.2	51.0	0.1

6.1.2 Pulse Test Results

As the Hukseflux gage results were nearly identical for each of the three pulse tests, only the detailed data from one pulse profile are presented. Figure 25 shows the gage heat flux as a function of the SCR power. It also shows the gage and cooling water return temperature.

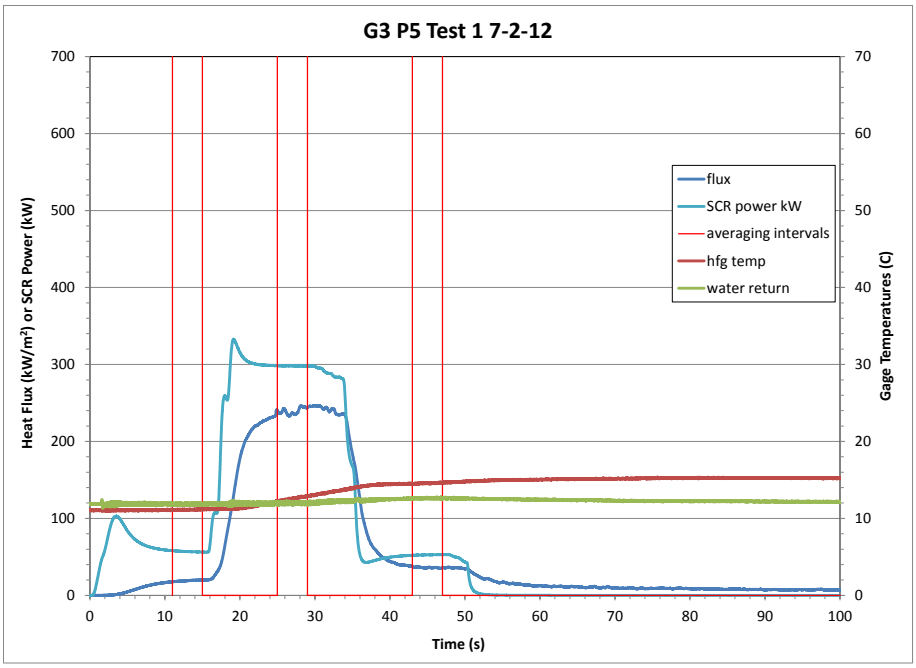

Figure 25 Representative Hukseflux Pulse Heat Flux and SCR Power

Figure 26 shows the SCR current and power for the Hukseflux gage test; the red line at 16 s indicates the end of the 10% step. Figure 27 presents the SCR voltage for the Hukseflux gage test.

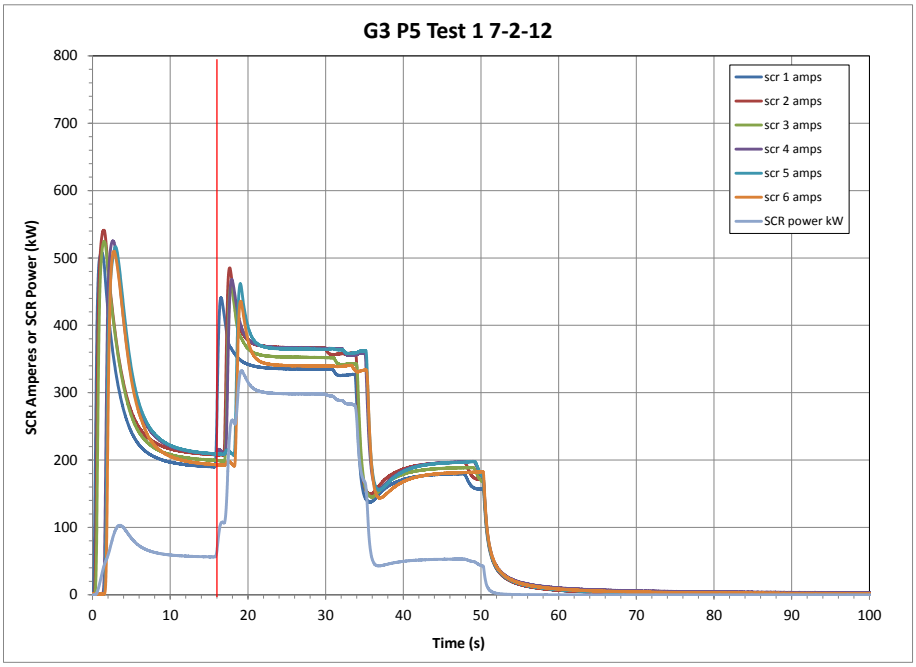

Figure 26 Representative Hukseflux Pulse SCR Current and Power

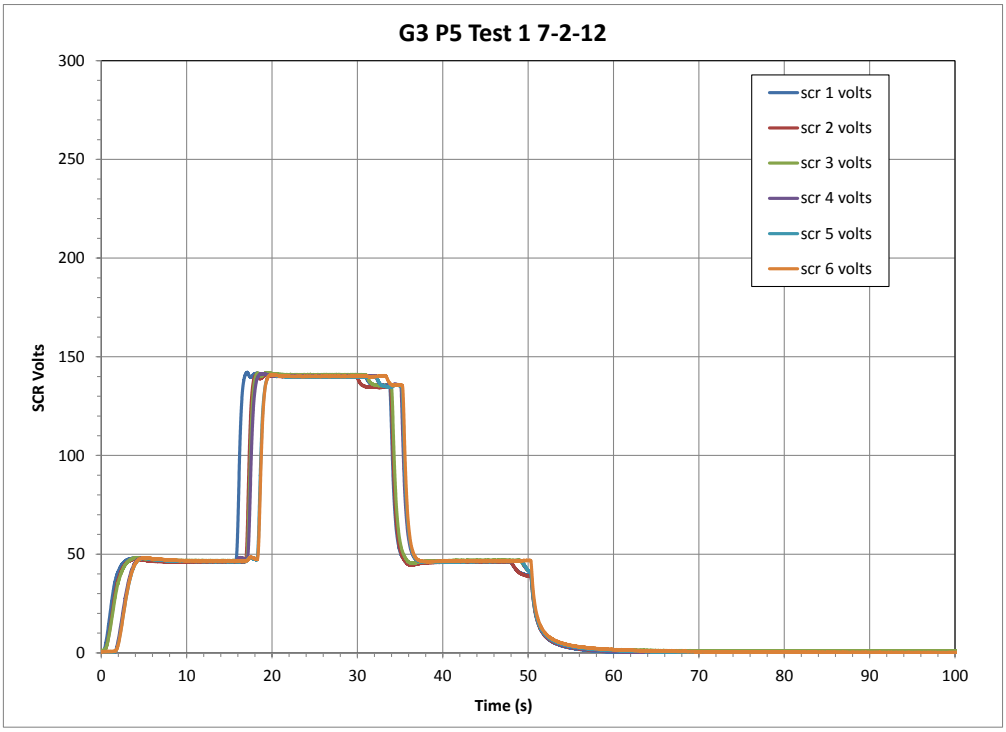

Figure 27 Representative Hukseflux Pulse SCR Voltage

Table 11 presents the heat flux and SCR power over each of the three averaging intervals.

Table 11 Hukseflux Representative Pulse Test

start s	stop s	end of step s	step	G3 P5 Test 1 7-2-12 SCR %	heat flux average kW/m2	1 std.dev.	SCR power average kW
11	15	16	1	10	19.0	0.7	57.0
25	29	30	2	30	239.2	4.1	298.3
43	47	48	3	10	36.1	0.6	52.6

Table 12 presents the average and standard deviation of the heat flux (in kW/m^2) and the SCR power (in kW) of the three Hukseflux gage pulse tests.

Table 12 Hukseflux Gage Average Results - Three Pulse Tests

G3 SCR %	G3 Pulse flux average	1 std.dev.	power average	1 std.dev.
10	18.6	0.7	57.5	0.9
30	240.2	2.9	297.5	0.7
10	36.6	0.7	52.4	0.2

7. DIRECTIONAL FLAME TEMPERATURE (DFT) HEAT FLUX SENSOR

A Directional Flame Temperature (DFT) fabricated by Org. 1532, measured absorbed heat flux.

The DFT construction consisted of two thin (3 inch x 3 inch, 0.1225 inch thick) Inconel (RA600 16ga ASTM B 168 HT) plates sandwiching a 1 inch thick piece of Cerablanket (Kaowool - 8PCF nominal density (128 kg/m^3)) using stainless steel (SS) all thread rod. The 1-inch thick Cerablanket was compressed to ¾-inch using SS standoffs in the all thread between the Inconel plates, yielding an effective insulation density of 170.7 kg/m^3 (nominal x1.333). See Appendix A for material thermal properties.

A typical DFT assembly usually has two MIMS type-K thermocouples attached to the inside center of each plate; the fielded DFT (shown in Figure 28) had five TCs (0.04 inch OD) attached to the inside of top plate (to access for 2D thermal conduction effects) and one TC attached to the inside of the bottom plate. Thin SS shim stock straps were welded over the tip of each TC; with TC1 centered, and TC2 and TC3 in a vertical direction and TC4 and TC5 in a horizontal direction, with 0.5 inch spacing between each TC.

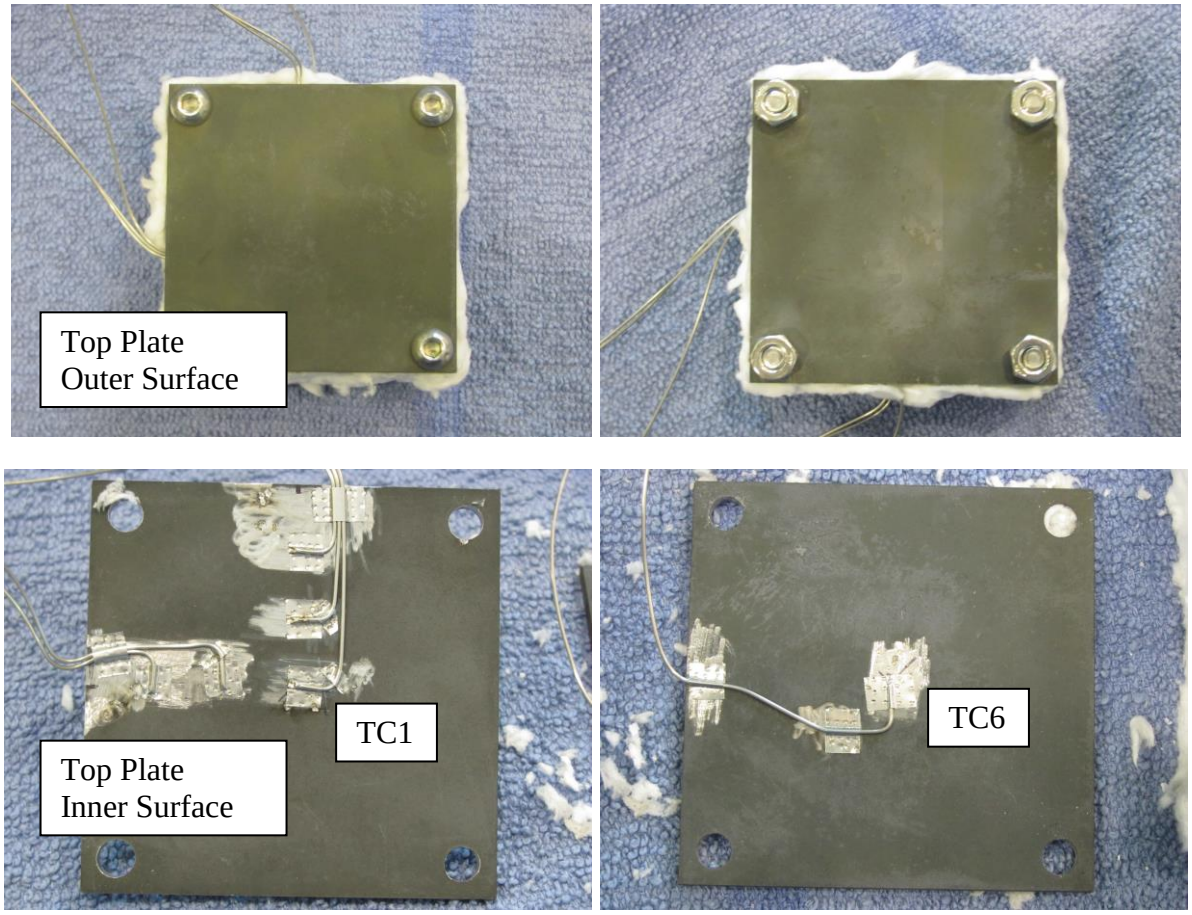

Figure 28 Min-DFT Assembly, Outside and Inside Front and Back Plate Views

To obtain a uniform emissivity, the plates were first cleaned with acetone, then baked at 1000^{0}C for one hour. The post bake emissivity of the DFT top plate outer surface was measured with a SOC-410C Handheld FTIR Reflectometer, yielding an emissivity of 0.603 ± 0.005. At the end of the test series, the DFT top plate outer surface emissivity was determined to be 0.624 ± 0.004. The DFT front (or top) plate, shown in Figure 29, was mounted flush with the insulated board surface.

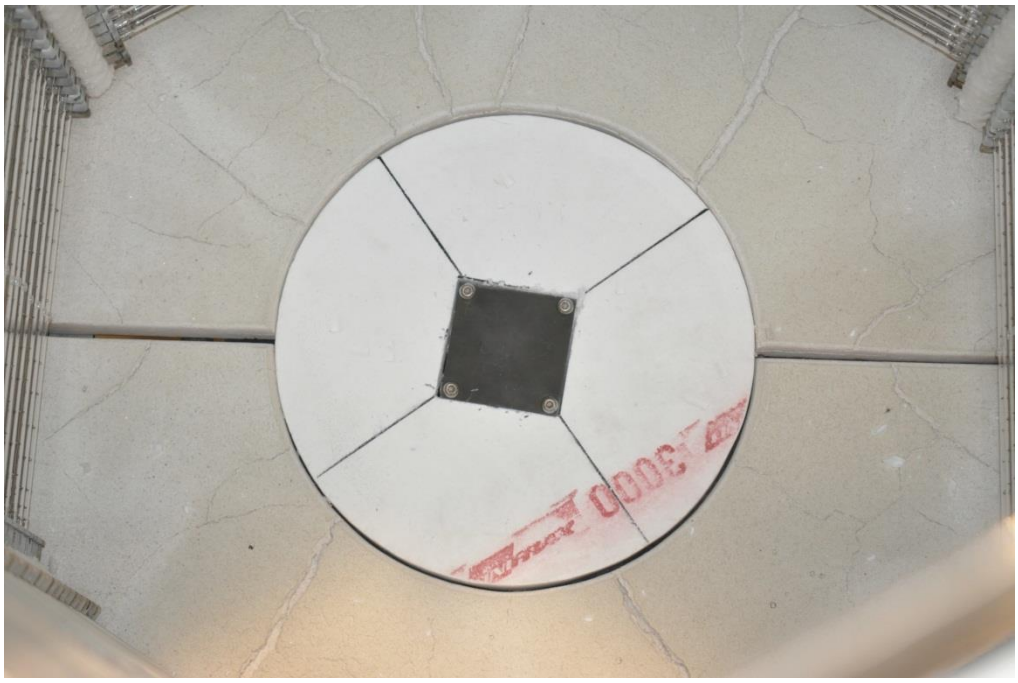

Figure 29 DFT Mounted inside the 6-Panel Array

The temperature response of the plate, along with the assumption of 1-dimensional conduction and an insulated back surface allows one to use two methods to estimate the net flux to the surface from the TC measurements. Data reduction can be performed using either the Excel macro developed for the Sandia Heat Flux Gage (SNL-HFG) (Blanchat et al. 2005) or by use of an inverse heat conduction code called "Inverse Heat Conduction Program 1-Dimensional (IHCP1D) (Version 7.0) (Beck 1999). Other inverse heat-conduction programs are available, e.g., Sandia One Dimensional Direct and Inverse Thermal program (SODDIT) (Blackwell et al. 1980), but IHCP1D was chosen because it is commercially available, has a graphical user interface (GUI), and can be used on an IBM-compatible personal computer.

Input parameters of an inverse heat conduction program are wall thickness, thermal conductivity, and volumetric heat capacity; insulation thickness, thermal conductivity, and volumetric heat capacity, boundary conditions, temperature sampling period; and numerical inputs. One-dimensional heat transfer was assumed in all cases.

V. F. Figueroa (2005) determined how uncertainties in temperature measurements, material geometries, material properties, or code-input parameters can affect the estimation of heat flux when using an inverse heat conduction code. Results of the analysis showed that the most important parameters were temperature uncertainty (Nakos 2004), the surface metal thickness and volumetric heat capacity. The use of a constant thermal properties rather than temperature dependent values also made a significant

difference in the resultant heat flux; therefore, temperature-dependent values should be used. The analysis determined a 15-19% uncertainty to 95% confidence when using inverse heat conduction methods, neglecting multidimensional effects.

IHCP returns the net flux at the surface and the surface temperature. The radiative heat flux (kW/m^2) is computed from the IHCP-calculated surface temperature (= ε x 5.67e-11 x $T_{surface}^4$). Eq. (1) shows the incident heat flux at the surface is calculated by dividing the sum of the net flux and the radiative flux by the surface absorptivity (α) which is assumed equal to the measured surface emissivity (ε = 0.624).

$$q_{incident} = (q_{net} + \varepsilon\sigma T_{surface}^{4}) / \alpha \qquad \text{Eq. 1}$$

7.1 DFT Test Results

7.1.1 Step Test Results

As the DFT gage results were nearly identical for each of the three step tests, only the detailed data from one step profile are presented. Figure 30 shows the gage heat flux as a function of the SCR power. The SCR step power profile was limited to 40% due to the high temperatures seen on the DFT. Figure 31 shows the gage temperatures (Top 4 thermocouple failed).

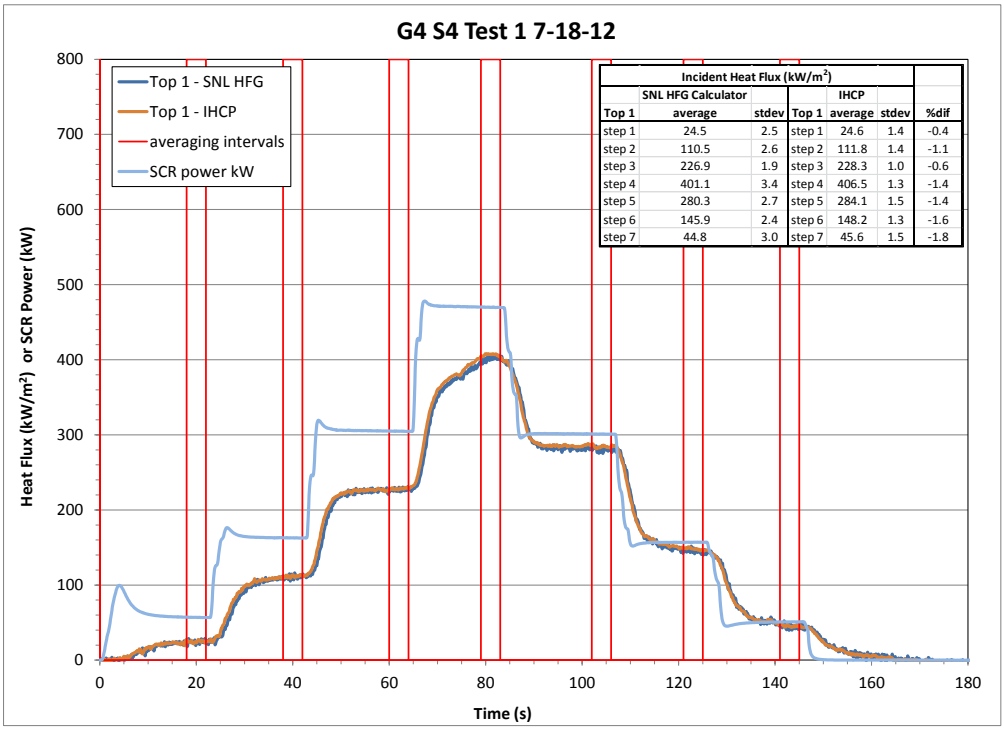

Incident Heat Flux (kW/m^2)						
	SNL HFG Calculator			IHCP		
Top 1	average	stdev	Top 1	average	stdev	%dif
step 1	24.5	2.5	step 1	24.6	1.4	-0.4
step 2	110.5	2.6	step 2	111.8	1.4	-1.1
step 3	226.9	1.9	step 3	228.3	1.0	-0.6
step 4	401.1	3.4	step 4	406.5	1.3	-1.4
step 5	280.3	2.7	step 5	284.1	1.5	-1.4
step 6	145.9	2.4	step 6	148.2	1.3	-1.6
step 7	44.8	3.0	step 7	45.6	1.5	-1.8

Figure 30 Representative DFT Gage Step Heat Flux and SCR Power

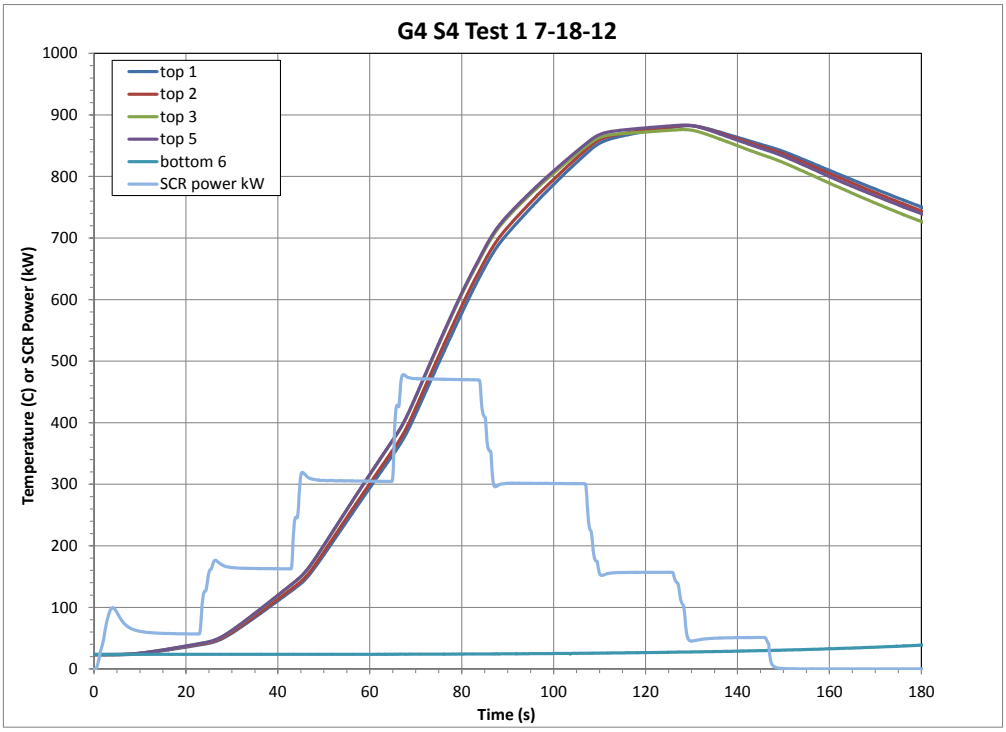

Figure 31 Representative DFT Gage Step Test Temperatures

Figure 32 shows the SCR current and power for the DFT gage test; the red line at 21 s indicates the end of the 10% step. Figure 33 presents the SCR voltage for the DFT gage test.

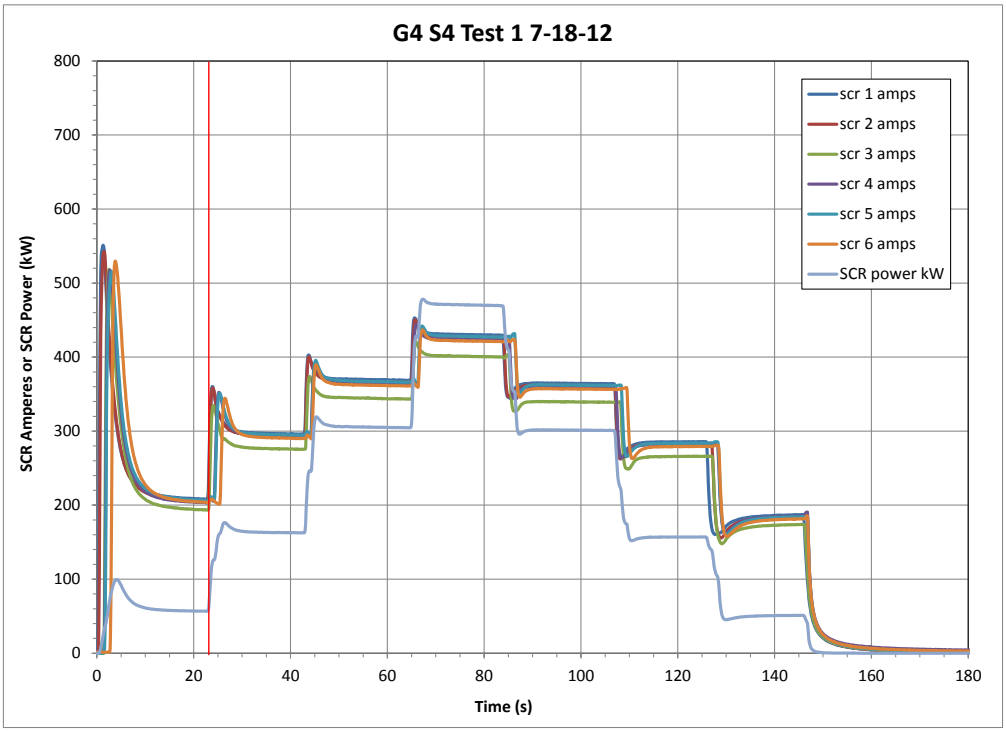

Figure 32 Representative DFT Gage Step SCR Current and Power

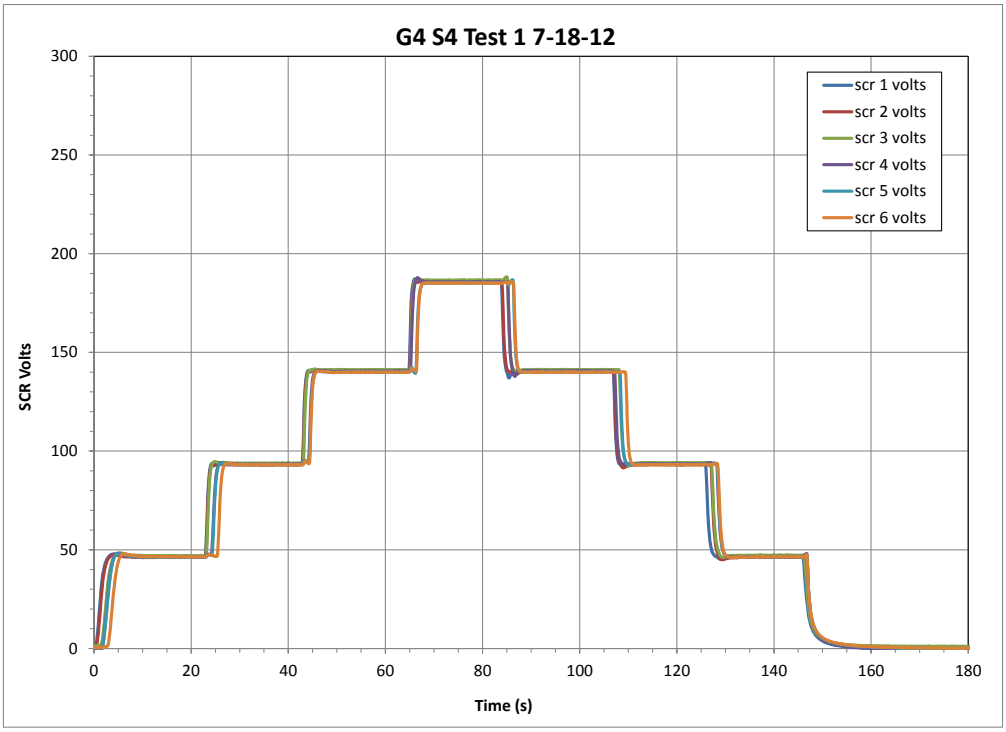

Figure 33 Representative DFT Gage Step SCR Voltage

Table 13 presents the heat flux and SCR power over each of the five averaging intervals.

Table 13 DFT Gage Representative Step Test

start	stop	end of step	step	G4 S4 Test 1 7-18-12 SCR %	average	1 std.dev.	SCR power average kW
18	22	23	1	10	24.6	1.4	24.6
38	42	43	2	20	111.8	1.4	111.8
60	64	65	3	30	228.3	1.0	228.3
79	83	84	4	40	406.5	1.3	406.5
102	106	107	5	30	284.1	1.5	284.1
121	125	126	6	20	148.2	1.3	148.2
141	145	146	7	10	45.6	1.5	45.6

Table 14 presents the average and standard deviation of the heat flux (in kW/m^2) and the SCR power (in kW) of the three DFT gage step tests.

Table 14 DFT Gage Average Results - Three Step Tests

G4 SCR %	G4 Step flux average	1 std.dev.	power average	1 std.dev.
10	23.9	0.9	57.1	0.2
20	110.8	0.9	162.4	0.5
30	226.3	1.8	303.8	1.1
40	402.9	3.4	469.4	0.7
30	285.8	1.5	299.9	1.2
20	148.4	0.9	156.7	0.4
10	46.1	0.6	50.9	0.1

7.1.2 Pulse Test Results

As the DFT gage results were nearly identical for each of the three pulse tests, only the detailed data from one pulse profile are presented. Figure 34 shows the gage heat flux as a function of the SCR power. Figure 35 shows the gage plate temperatures.

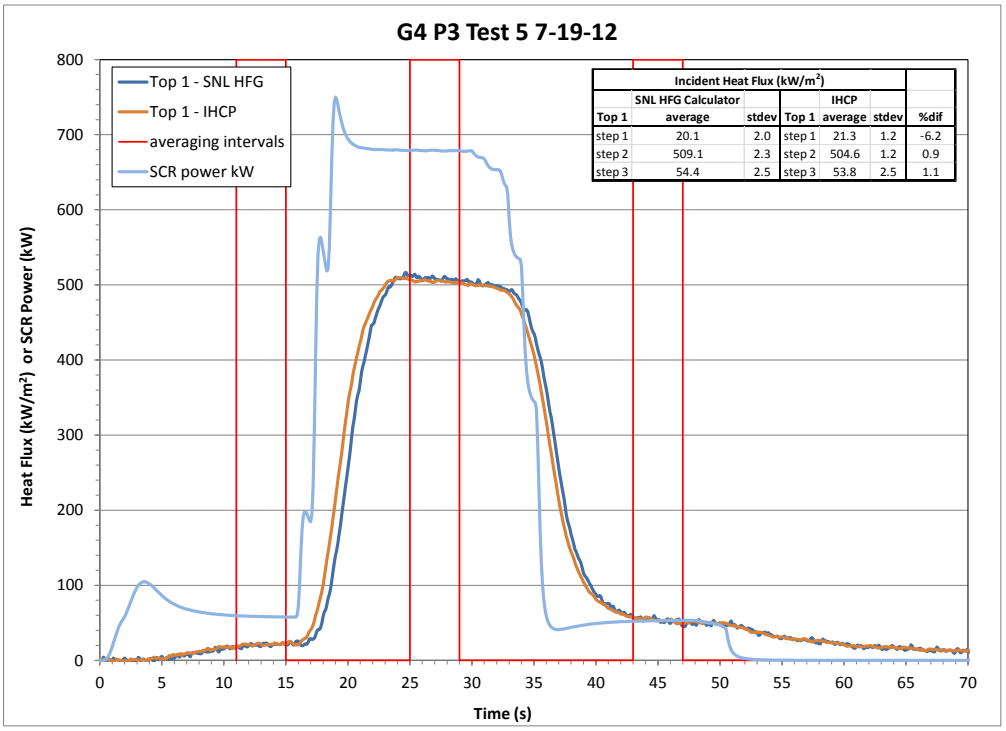

Figure 34 Representative DFT Pulse Heat Flux and SCR Power

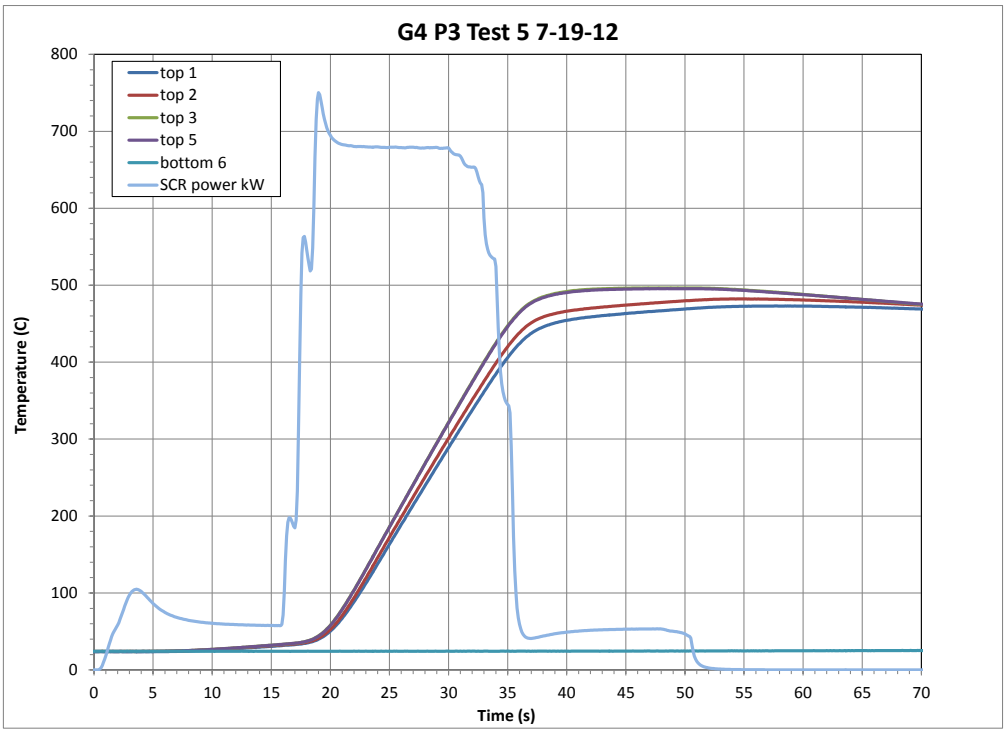

Figure 35 Representative DFT Temperatures

Figure 36 shows the SCR current and power for the DFT gage test; the red line at 16 s indicates the end of the 10% step. Figure 37 presents the SCR voltage for the DFT gage test.

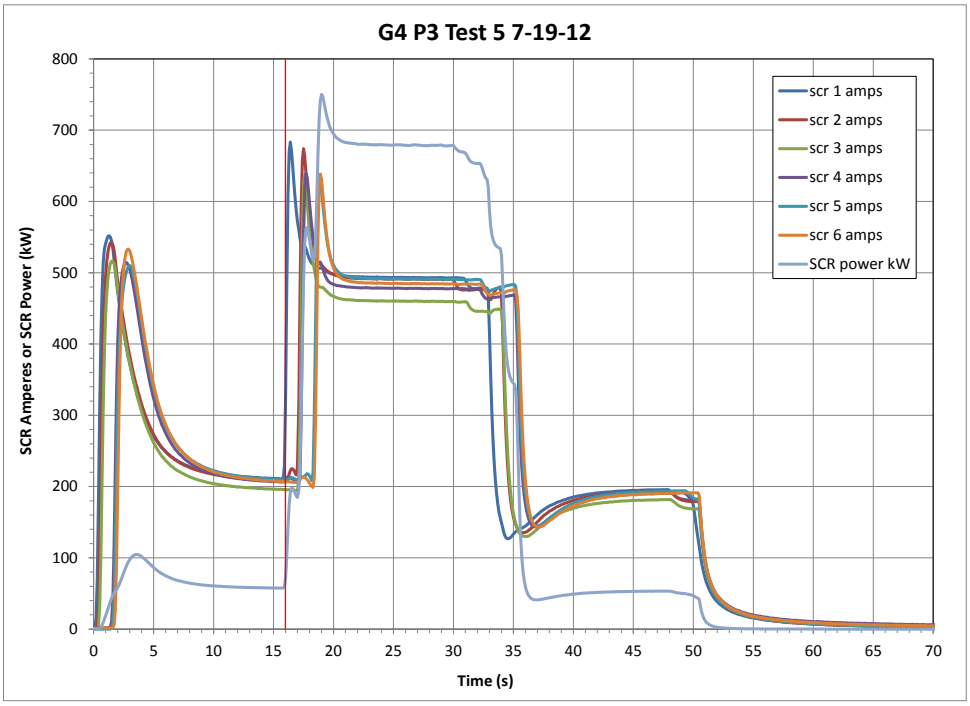

Figure 36 Representative DFT Pulse SCR Current and Power

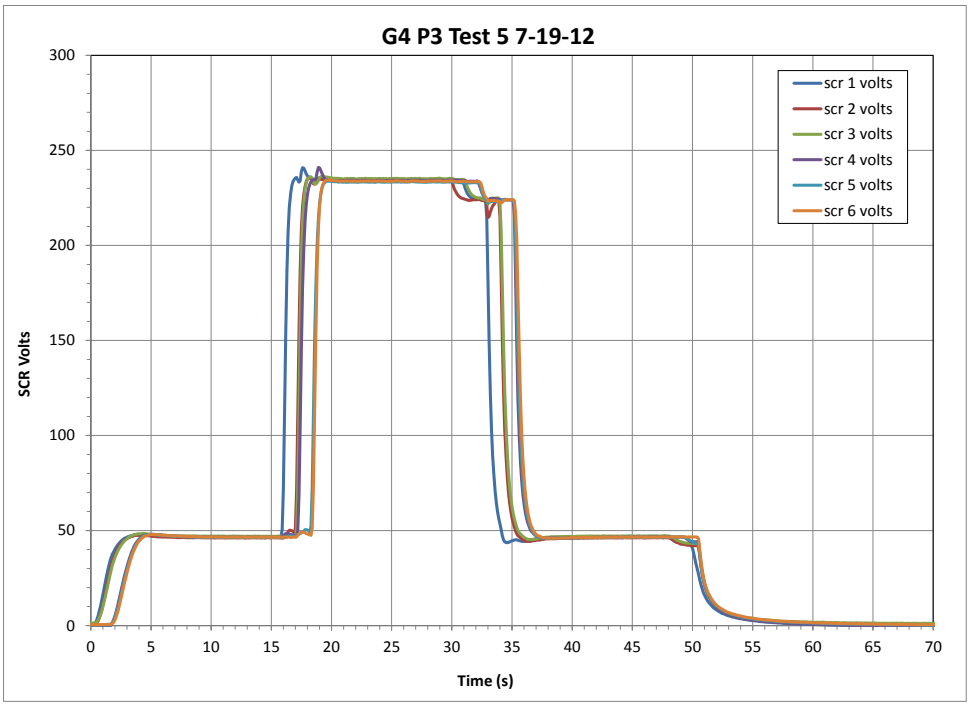

Figure 37 Representative DFT Pulse SCR Voltage

Table 15 presents the heat flux and SCR power over each of the three averaging intervals.

Table 15 DFT Representative Pulse Test

start	stop	end of step	step	G4 P3 Test 5 7-19-12 SCR %	average	1 std.dev.	SCR power average kW
11	15	16	1	10	21.3	1.2	58.5
25	29	30	2	50	504.6	1.2	678.9
43	47	48	3	10	53.8	2.5	52.9

Table 16 presents the average and standard deviation of the heat flux (in kW/m^2) and the SCR power (in kW) of the three DFT gage pulse tests.

Table 16 DFT Gage Average Results - Three Pulse Tests

G4 SCR %	G4 Pulse flux average	1 std.dev.	power average	1 std.dev.
10	18.0	0.1	59.4	0.9
50	503.7	0.6	678.2	0.7
10	54.7	0.0	52.6	0.3

8. HIGH TEMPERATURE HEAT FLUX SENSOR (HTHFS)

A high temperature heat flux sensor (HTHFS), shown in Figure 38, also measured total heat flux. The HTHFS, designed by Tom Diller (Virginia Tech), is based on the "transverse Seebeck coefficient" concept. The HTHFS was about 1 inch long x 0.5 inch wide x 1/8 inch thick. In this type of gage the temperature difference is generated in the same direction as the incoming flux (vertical in this case), same as other types of flux gages, but the output voltage is generated horizontally. The HTHFS was formed from multiple layers of chromel and alumel sheets (stacked vertically) welded together at alternating top and bottom surfaces. The HTHFS was surface mounted and had no active cooling. Two type-K thermocouples provide a gage temperature measurement as well as a gage output measurement to infer incident heat flux. Raphael-Mabel et al. (2005) and Gifford et al. (2010) provide additional information about the transverse Seebeck coefficient concept and the HTHFS gage.

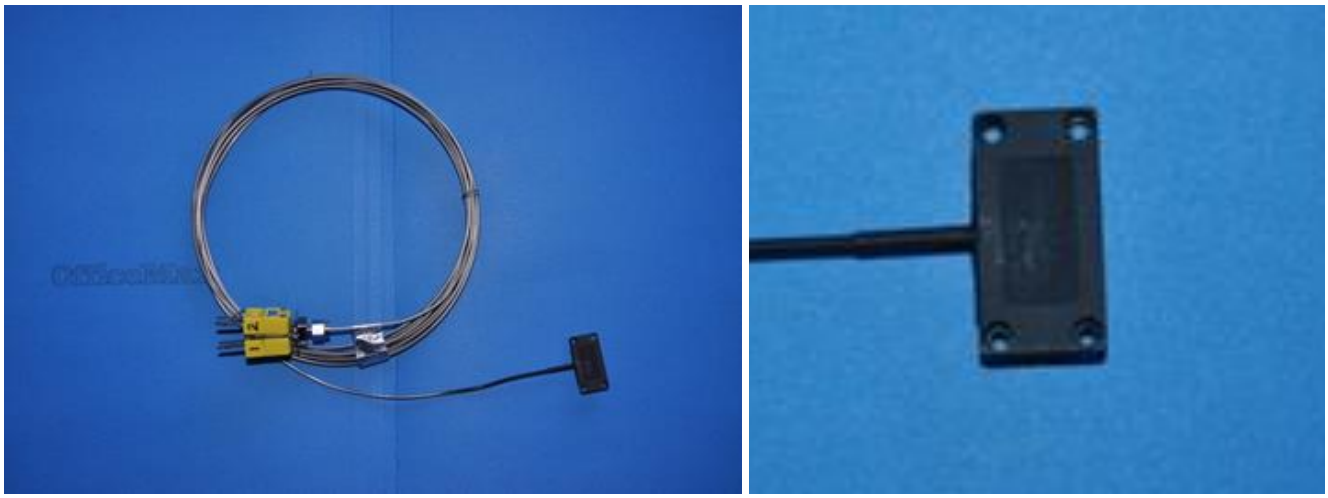

Figure 38 High Temperature Heat Flux Sensor (HTHFS)

The HTHFS, shown in Figure 39, was mounted to a stainless steel plate (as a heat sink), that in turn was flush mounted to the insulated board. It was screwed to the SS plate and bonded in place with a light coating of Cotronics high temperature (1650°C) alumina adhesive (#989). Two 0.040 inch OD MINS Type-K and one Type-N thermocouples were welded to the SS heat sink approximately 0.5 inches from the HTHFS.

The emissivity of a new HTHFS was determined to be 0. 86 ± 0.01, as measured with a 0.86 ± 0.01 SOC-410C Handheld FTIR Reflectometer (note that Appendix B states the surface absorptivity is 0.9). After repeated tests at high temperature, the surface emissivity was slighted reduced; the used gage emissivity was 0.83 ± 0.01. However, this value of emissivity may not be accurate for two reasons: 1) this is a difficult measure to make with this instrument due to the small surface area and 2) these measurements are taken at room temperature and the may be different at the high temperature seen in the tests.

Figure 39 HTHFS Mounted to Steel Plate with Additional Thermocouples

The HTHFS, shown in Figure 40, was mounted flush with the insulated board surface, facing upward.

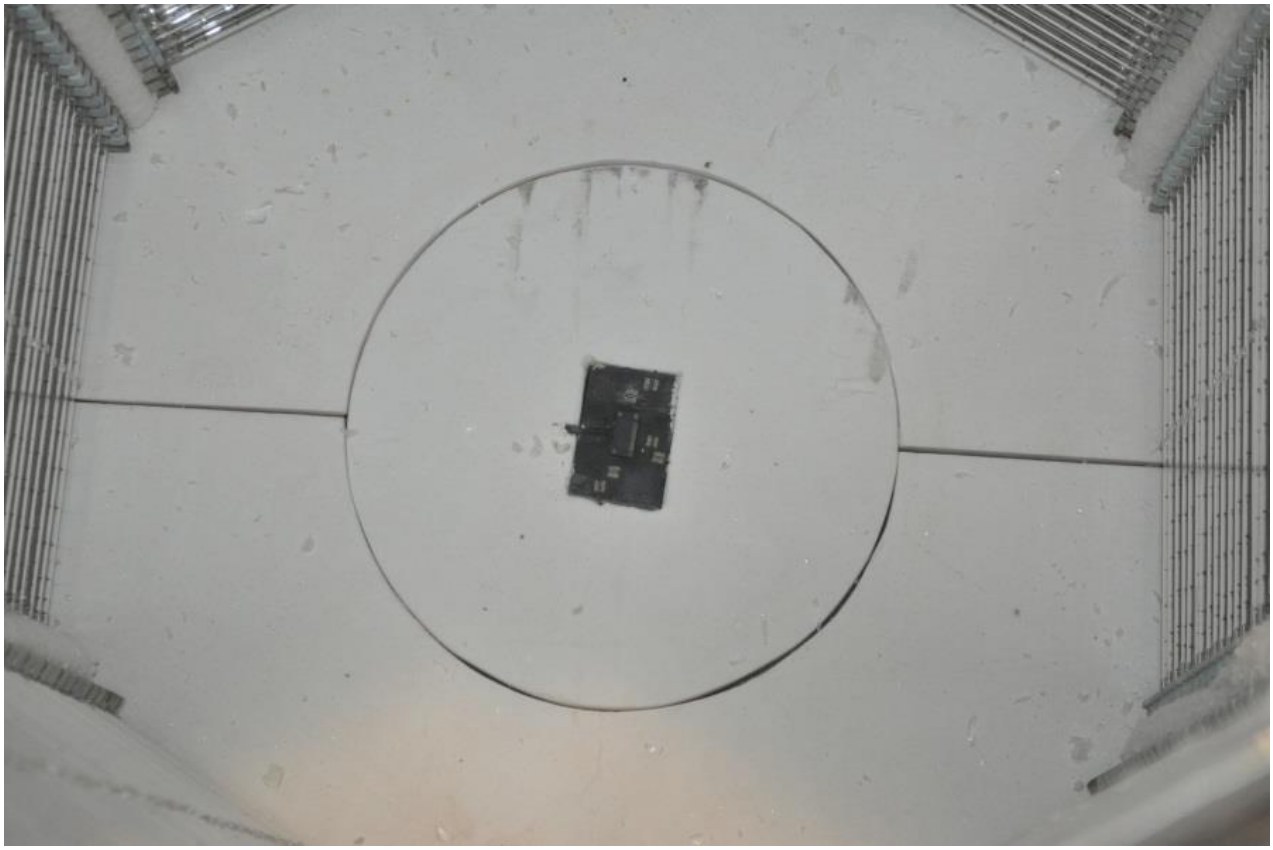

Figure 40 HTHFS Mounted inside the 6-Panel Array

HTHFS data reduction utilized the calibration documentation for the sensors delivered to Dept. 1532 on May 20, 2011 (see Appendix B) and an Excel spreadsheet routine developed by Tom Blanchat, Jim Nakos, and Tom Diller. The hybrid heat flux (HHF) data reduction methodology (Hubble and Diller 2010) was used to determine net (absorbed) flux. A radiation term was added to determine incident heat flux.

1. Record HTHFS front surface (T_1) and back surface (T_2) temperature and primary (Cr-Cr) voltage (V_{out}).

2. Determine and subtract bias voltage (if any) from baseline voltage.

3. Determine and apply the temperature correction factor, S(T), to the gage room temperature sensitivity, $S_1(25°C)$, to compute the gage differential flux in kW/m^2. (see Appendix B).

$$q''_{diff} = \frac{V_{out}}{S(T)}; \quad S(T) = S_1(25^\circ C) \times (AT^5 + BT^4 + CT^3 + DT^2 + ET + F)$$

Eq. 2

4. Calculate gage average temperature $T_{ave} = (T_1 + T_2)/2$.

5. Calculate gage time rate of change d/dt (T_{ave}). (Note: T_{ave} will typically be a noisy signal, and will need to be filtered prior to computing the differential.

6. Compute gage "slug" heat flux in kW/m^2. (note: measured $\rho c_p \delta$ = 1.3 J/cm^{2}K, see Appendix B)

$$q''_{slug} = \rho c_p \delta \frac{d}{dt}(T_{ave})$$

Eq.3

7. Compute gage net heat flux into the sensor face

$$q''_{net} = q''_{diff} + \frac{1}{2} q''_{slug}$$

Eq.4

8. Compute radiation term (radiation leaving the sensor face) (ε = 0.93 assumed, σ = 5.67e-11 kW/m^{2}K^4)

$$q''_{rad} = \varepsilon\sigma(T_1 + 273)^4$$

Eq.5

9. Compute gage incident heat flux (assumed ε = α = 0.83)

$$q''_{inc} = (q''_{net} + q''_{rad})/\alpha$$

Eq.6

8.1 HTHFS Test Results

8.1.1 Step Test Results – Gage 6

The HTHFS gage 6 (sensor #1 in Appendix B) heat flux results were similar but not quite identical for each of the three step tests, as discussed later. However, for comparison with the previous measurements, only the detailed data from one step profile are presented. Figure 41 shows the gage heat flux as a function of the SCR power. Figure 42 shows the gage temperatures.

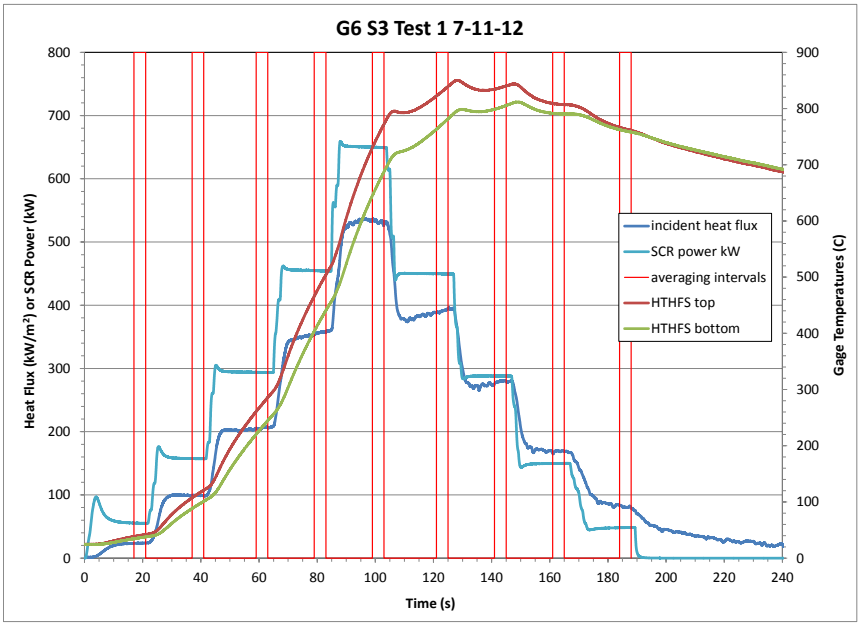

Figure 41 Representative HTHFS Gage 6 Step Heat Flux and SCR Power

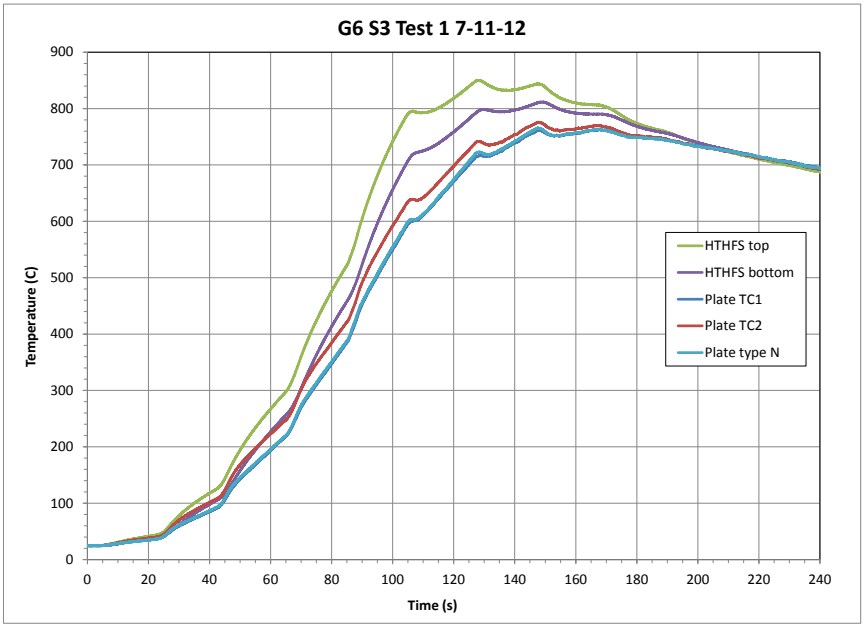

Figure 42 Representative HTHFS Gage Step Test Temperatures

Figure 43 shows the SCR current and power for the HTHFS gage test; the red line at 65 s indicates the end of the 30% step. Figure 44 presents the SCR voltage for the HTHFS gage test.

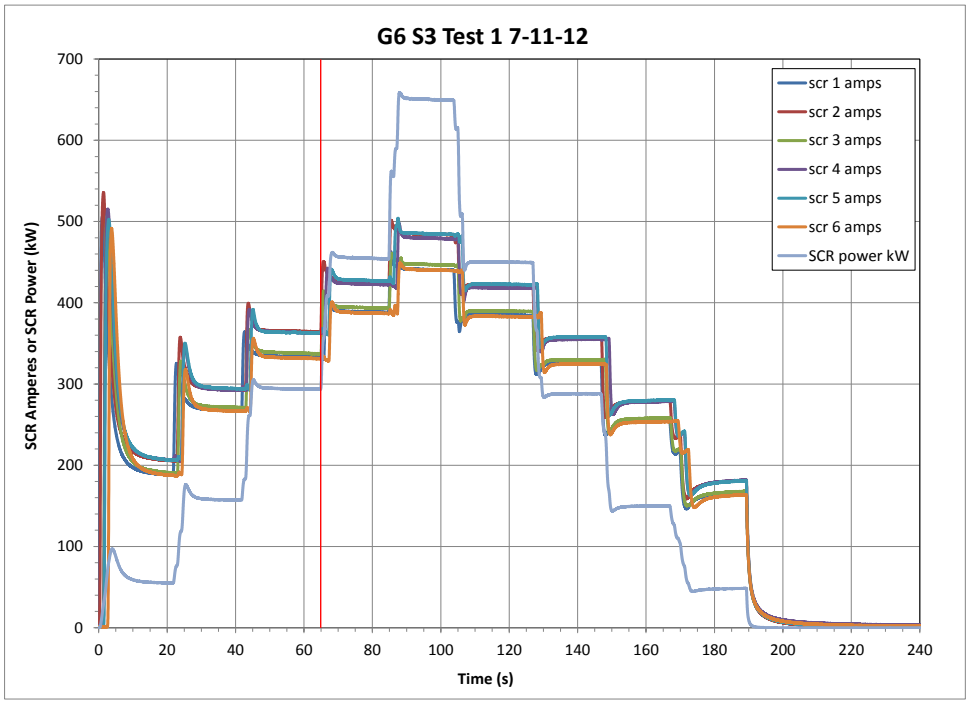

Figure 43 Representative HTHFS Gage Step SCR Current and Power

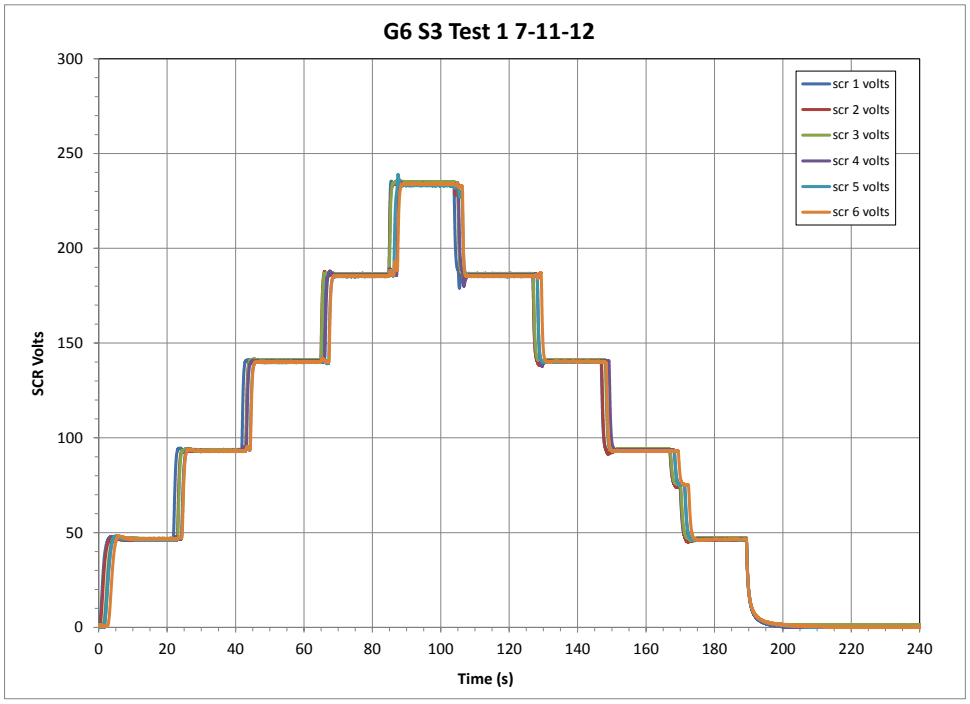

Figure 44 Representative HTHFS Gage Step SCR Voltage

Table 17 through Table 19 presents the heat flux and SCR power for the three Gage 6 sensor tests over each of the nine averaging intervals.

Table 17 HTHFS Gage 6 Step Test 1

start s	stop s	end of step s	step	G6 S3 Test 1 7-11-12 SCR %	heat flux average kW/m2	1 std.dev.	SCR power average kW
17	21	22	1	10	23.7	0.2	55.2
37	41	42	2	20	99.1	0.2	157.3
59	63	64	3	30	205.8	1.4	293.8
79	83	84	4	40	357.0	1.5	454.5
99	103	104	5	50	532.0	2.4	649.6
121	125	126	6	40	391.6	2.3	449.7
141	145	146	7	30	279.3	1.1	288.1
161	165	166	8	20	168.9	1.2	149.8
184	188	189	9	10	80.5	1.8	48.2

Table 18 HTHFS Gage 6 Step Test 2

start s	stop s	end of step s	step	G6 S3 Test 2 7-11-12 SCR %	heat flux average kW/m2	1 std.dev.	SCR power average kW
18	22	23	1	10	21.9	0.1	55.0
37	41	42	2	20	90.9	0.4	157.1
60	64	65	3	30	190.9	1.0	293.0
79	83	84	4	40	333.3	1.4	454.6
100	104	105	5	50	490.3	2.0	648.4
123	127	128	6	40	368.7	2.5	448.4
142	146	147	7	30	261.9	2.2	285.8
162	166	167	8	20	158.1	1.0	149.2
184	188	189	9	10	76.4	2.0	48.0

Table 19 HTHFS Gage 6 Step Test 3

start s	stop s	end of step s	step	G6 S3 Test 3 7-12-12 SCR %	heat flux average kW/m2	1 std.dev.	SCR power average kW
17	21	22	1	10	20.2	0.1	54.8
37	41	42	2	20	86.8	0.4	156.7
59	63	64	3	30	181.1	0.7	292.9
79	83	84	4	40	319.0	0.8	452.4
102	106	107	5	50	475.7	1.9	647.2
121	125	126	6	40	348.3	2.7	446.7
141	145	146	7	30	248.4	1.8	285.3
161	165	166	8	20	148.9	1.5	148.5
183	187	188	9	10	69.3	2.6	47.7

Figure 45 presents the average heat flux (in kW/m^2) for the three Gage 6 step tests, calculated at each 10% power step interval as the SCR power is ramped up to 50% power and then back to 10% power. There was an 8-10% difference in Test 2 and Test 3 (decrease) from that seen in Test 1. Since the change in emissivity between pre- and post-test was not significant, the cause was thought to be an issue with the attachment to the mounting plate, possibly a change in the Cotronix property as it cured during the test. Note that extensive thermal cycling tests to 1000°C performed in a kiln and with a propane torch by Gifford et al. (2010) showed no appreciable shift in gage sensitivity. However, Dr. Diller has noted that the paint coating does not usually survive tests at high temperature, and the gage will oxidize

to a lower emissivity. Note that a lower emissivity would result in a higher incident heat flux measurement (while not affecting the gauge sensitivity).

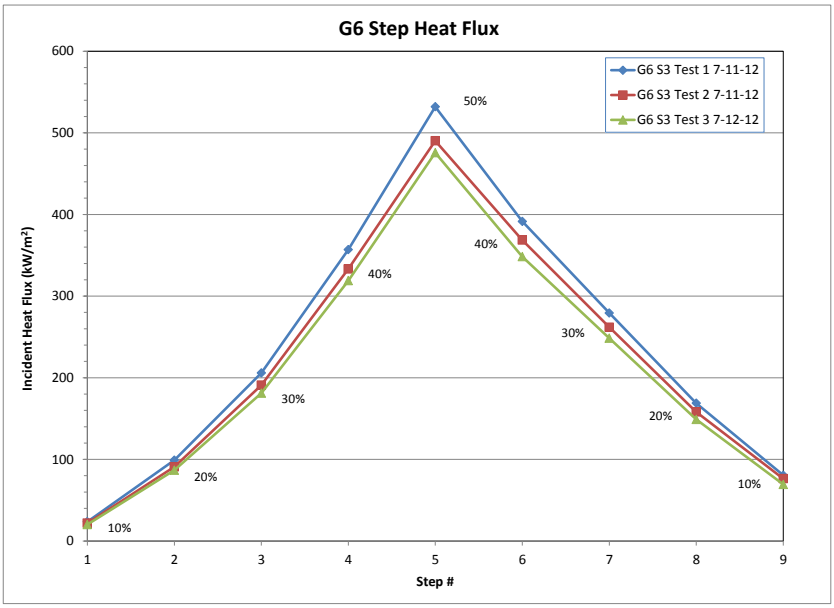

Figure 45 HTHFS Gage 6 Step Test Series Flux Comparison

Table 20 presents the average and standard deviation of the heat flux (in kW/m^2) and the SCR power (in kW) of the three HTHFS Gage 6 step tests.

Table 20 HTHFS Gage 6 Average Results - Three Step Tests

G6 SCR %	G6 Step flux average	1 std.dev.	power average	1 std.dev.
10	21.9	1.7	55.0	0.2
20	92.3	6.3	157.0	0.3
30	192.6	12.5	293.2	0.5
40	336.4	19.2	453.8	1.2
50	499.3	29.2	648.4	1.2
40	369.5	21.6	448.3	1.5
30	263.2	15.5	286.4	1.5
20	158.6	10.0	149.2	0.7
10	75.4	5.7	48.0	0.3

8.1.2 Step Test Results – Gage 6a

After cleaning the lamp panels and replacing a few blown lamps, a second HTHFS step test series was performed. The HTHFS gage 6a (sensor #2 in Appendix B) was prepared and mounted to the plate (with a thin layer of Cotronix ceramic paste). As before, the heat flux results were not identical for each of the replicate step tests. Table 21 through Table 24 present the heat flux and SCR power for the four Gage 6a sensor tests over each of the nine averaging intervals. Prior to Test 4, Gage 6a was removed from the plate, the plate was cleaned, and the gage remounted with fresh Cotronix ceramic. During removal, it

was noted that the thin disk of Cotronix cement had hardened and fell freely from the plate (possibly indication of a thermal gap).

Table 21 HTHFS Gage 6a Step Test 1

start s	stop s	end of step s	step	G6a S3 Test 1 7-26-122 SCR %	heat flux average kW/m2	1 std.dev.	SCR power average kW
17	21	22	1	10	25.6	0.2	56.7
37	41	42	2	20	111.7	0.2	161.8
59	63	64	3	30	218.5	1.5	302.4
80	84	85	4	40	368.3	3.6	468.2
100	104	105	5	50	545.9	2.3	667.1
120	124	125	6	40	391.8	1.0	462.4
142	146	147	7	30	268.9	1.0	294.9
162	166	167	8	20	160.3	1.6	153.8
185	189	190	9	10	70.0	1.4	49.6

Table 22 HTHFS Gage 6a Step Test 2

start s	stop s	end of step s	step	G6a S3 Test 2 7-26-12 SCR %	heat flux average kW/m2	1 std.dev.	SCR power average kW
17	21	22	1	10	21.6	0.2	56.7
37	41	42	2	20	90.8	0.3	161.7
60	64	65	3	30	182.2	1.4	302.1
79	83	84	4	40	314.9	1.3	467.5
99	103	104	5	50	462.8	1.2	667.7
119	123	124	6	40	347.2	1.5	462.9
142	146	147	7	30	244.8	3.6	295.5
162	166	167	8	20	148.3	0.8	154.2
183	187	188	9	10	68.1	0.9	49.7

Table 23 HTHFS Gage 6a Step Test 3

start s	stop s	end of step s	step	G6a S3 Test 3 7-27-12 SCR %	heat flux average kW/m2	1 std.dev.	SCR power average kW
17	21	22	1	10	20.5	0.1	56.6
37	41	42	2	20	86.2	0.3	161.5
59	63	64	3	30	176.8	0.7	302.0
79	83	84	4	40	307.8	1.4	467.4
99	103	104	5	50	457.7	1.6	668.6
121	125	126	6	40	342.8	1.7	461.6
141	145	146	7	30	238.5	0.9	294.7
163	167	168	8	20	139.8	1.1	153.9
185	189	190	9	10	61.1	0.6	49.8

Table 24 HTHFS Gage 6a Step Test 4

start s	stop s	end of step s	step	G6a S3 Test 4 8-1-12 SCR %	heat flux average kW/m2	1 std.dev.	SCR power average kW
17	21	22	1	10	19.5	0.2	56.5
37	41	42	2	20	81.6	0.1	160.5
57	61	62	3	30	164.2	0.3	300.4
77	81	82	4	40	281.8	1.8	464.0
100	104	105	5	50	450.8	2.0	663.1
120	124	125	6	40	329.0	1.6	457.9
143	147	148	7	30	226.6	2.2	292.5
163	167	168	8	20	129.0	1.6	152.3
185	189	190	9	10	54.5	0.8	49.2

Figure 46 presents the average heat flux (in kW/m^2) for the four Gage 6a step tests, calculated at each 10% power step interval as the SCR power is ramped up to 50% power and then back to 10% power. There was an ~15% difference in Test 2, Test 3, and Test 4 (decrease) from that seen in Test 1. Note that results in Test 4 were expected to be similar to Test 1, based on the gauge remount with a fresh coat of Cotronix. Also, greater decreases were seen in the Gauge 6a test series (after the first test) as compared to the Gauge 6 tests. The cause of the differences are being investigated.

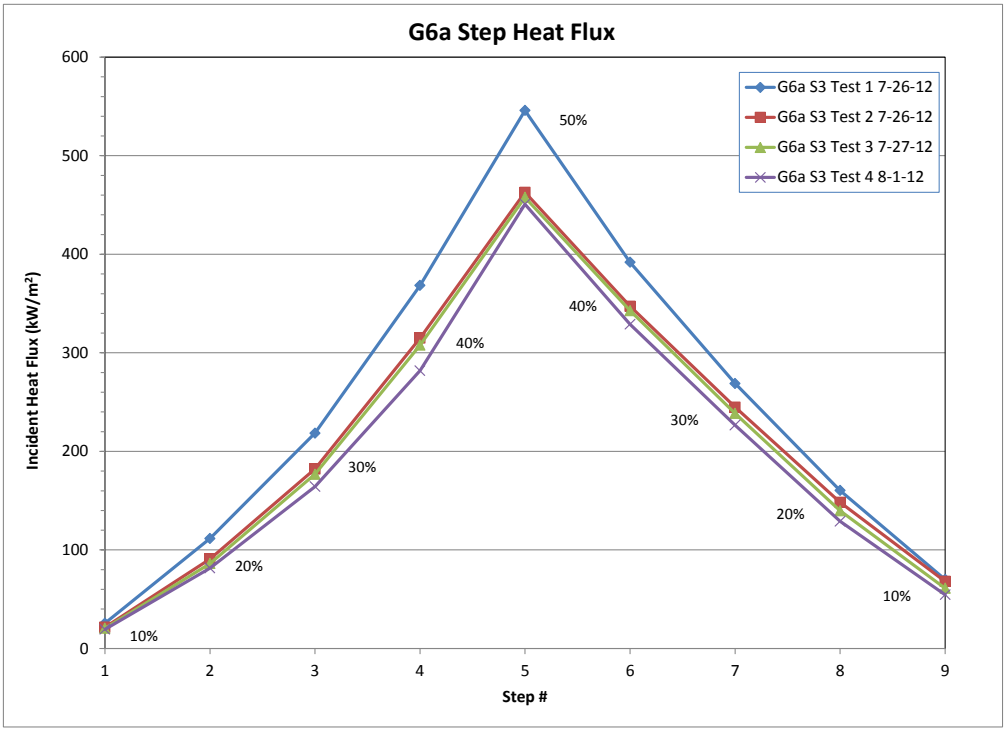

Figure 46 HTHFS Gage 6a Step Test Series Flux Comparison

Table 25 presents the average and standard deviation of the heat flux (in kW/m^2) and the SCR power (in kW) of the four HTHFS Gage 6a step tests. Note that the SCR power average was ~1-2% greater than in previous tests due to the cleaning and panel relamping.

Table 26 provides the average power (kW) and standard deviation for all gages in all step tests, indicating very little difference between tests.

Table 25 HTHFS Gage 6a Average Results - Four Step Tests

G6a SCR %	G6a Step flux average	1 std.dev.	power average	1 std.dev.
10	21.8	2.7	56.6	0.1
20	92.6	13.3	161.4	0.6
30	185.4	23.3	301.7	0.9
40	318.2	36.3	466.8	1.9
50	479.3	44.7	666.7	2.4
40	352.7	27.2	461.2	2.3
30	244.7	17.8	294.4	1.3
20	144.4	13.3	153.5	0.9
10	63.4	7.1	49.6	0.3

As noted, an interesting effect was seen in repeated high temperature tests with the High Temperature Heat Flux Sensor (HTHFS), with a decrease in heat flux in tests subsequent to the initial test. Figure 47 clearly shows this effect. New gages have been ordered in order to perform additional tests and determine the cause of the flux reduction.

We also have determined that gauges are mounted (in calibrations at Virginia Tech) using a high temperature aluminum nitride adhesive, which forms a thin (0.01 cm) bond line between the hot plate base and the sensor/faceplate in order to reduce thermal contact resistance. This method of mounting will be explored in future tests.

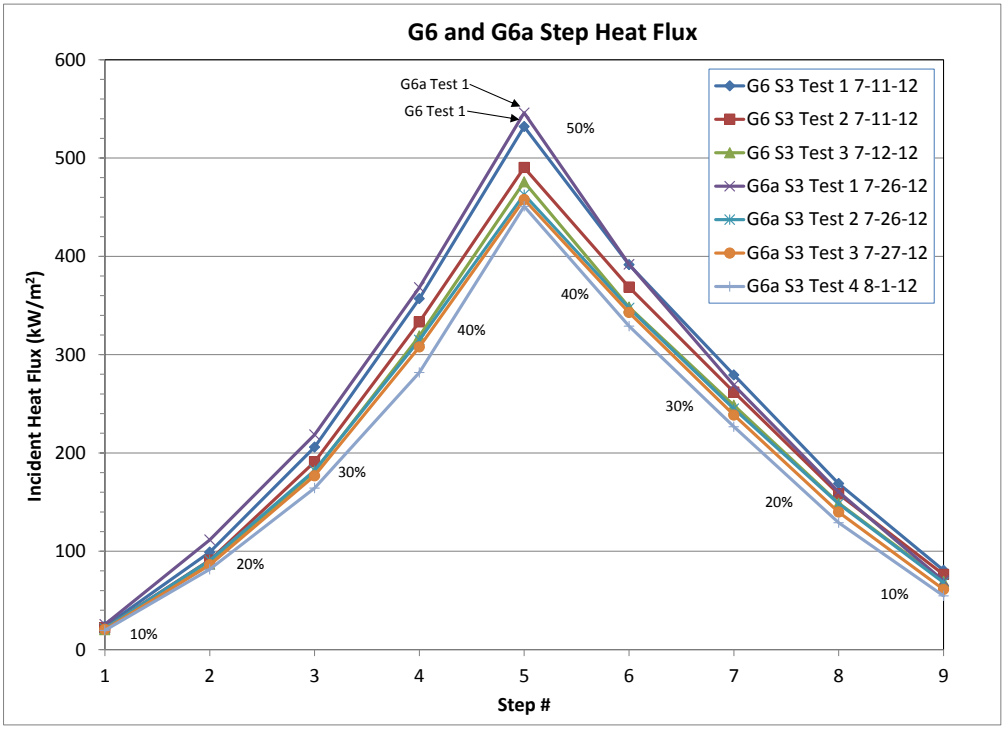

Figure 47 HTHFS Gage 6 and Gage 6a - Heat Flux Comparison - Step Tests

Table 26 Average and S.D. of SCR Power (all gages in all step tests)

SCR %	power average (all step tests)	1 std.dev.
10	55.9	0.8
20	159.7	2.0
30	298.8	3.9
40	462.6	6.0
50	658.7	7.6
40	458.2	7.8
30	293.4	4.5
20	153.1	2.7
10	49.5	1.2

8.1.3 Pulse Test Results – Gage 6

The pulse test was only performed using Gage 6. Note that this test series was performed before the Gage 6 step tests; the maximum gage temperature was ~400°C. As the HTHFS gage results were nearly identical for each of the three pulse tests, only the detailed data from one pulse profile are presented. Figure 48 shows the gage heat flux as a function of the SCR power. It also shows the gage temperature. Figure 49 shows the plate and gage temperatures.

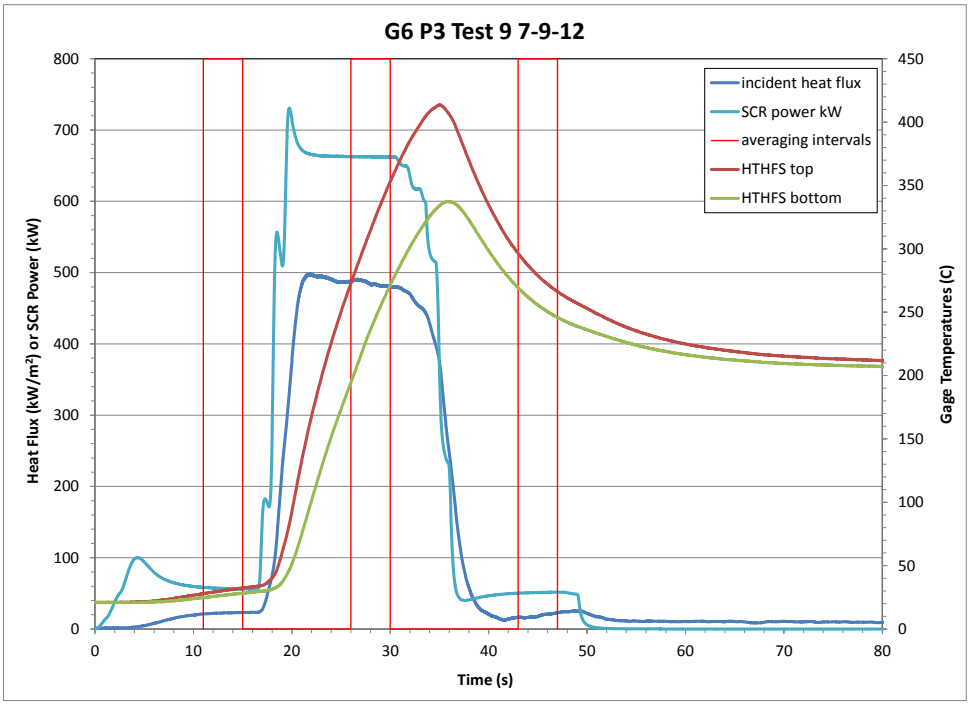

Figure 48 Representative HTHFS Gage 6 Pulse Test Heat Flux and SCR Power

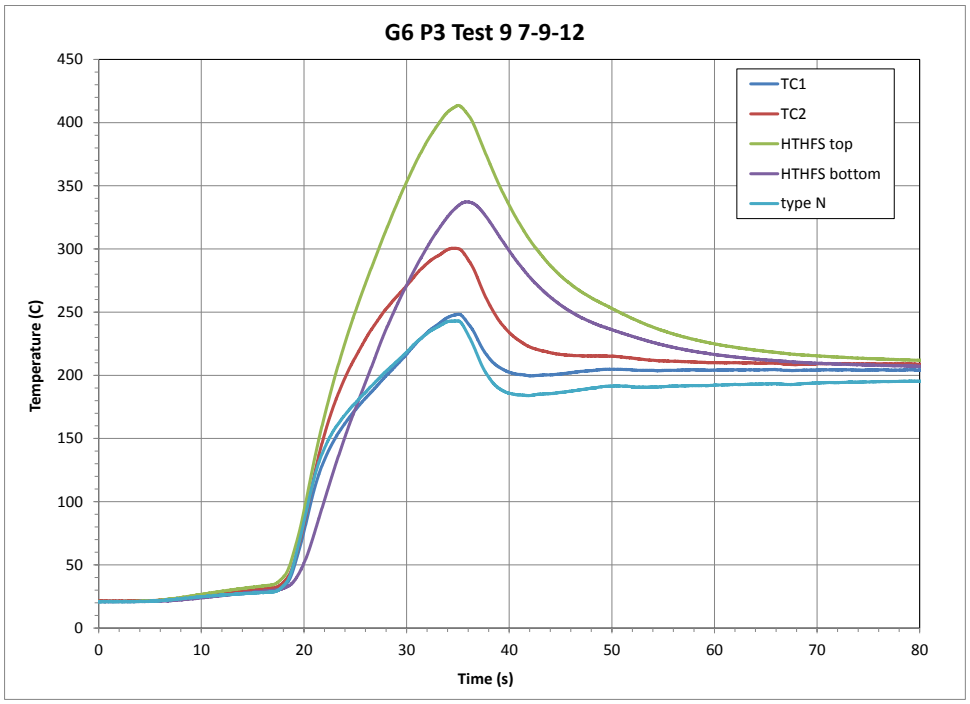

Figure 49 Representative HTHFS Gage 6 Pulse Test Temperatures

Figure 50 shows the SCR current and power for the HTHFS gage test; the red line at 31 s indicates the end of the 50% step. Figure 51 presents the SCR voltage for the HTHFS gage test.

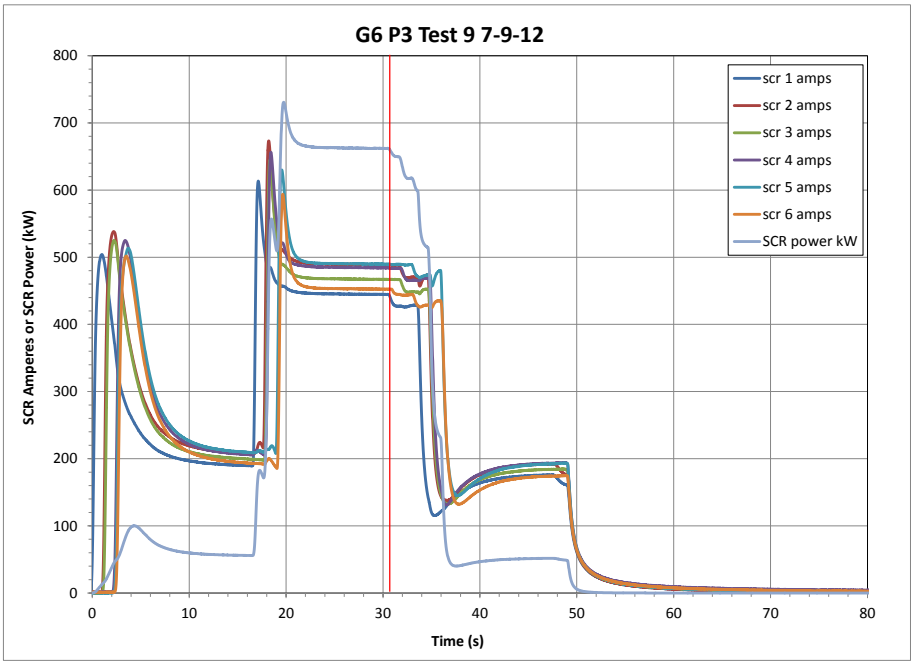

Figure 50 Representative HTHFS 6 Pulse Test SCR Current and Power

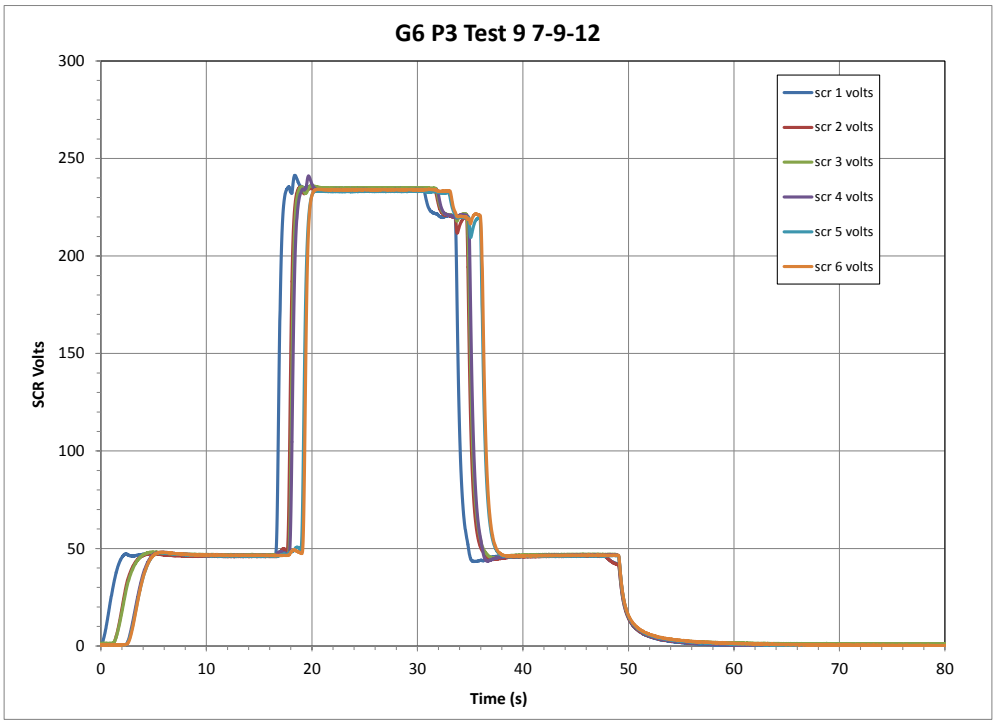

Figure 51 Representative HTHFS 6 Pulse Test SCR Voltage

Table 27 presents the heat flux and SCR power over each of the three averaging intervals.

Table 27 HTHFS Gage 6 Representative Pulse Test Heat Flux

start s	stop s	end of step s	step	G6 P3 Test 9 7-9-12 SCR %	heat flux average kW/m2	1 std.dev.	SCR power average kW
11	15	16	1	10	22.4	0.6	57.1
26	30	31	2	50	485.0	3.4	662.4
43	47	48	3	10	18.6	2.3	51.1

Figure 52 and Table 28 presents the average heat flux (in kW/m^2) for the three Gage 6 pulse tests, calculated at each step interval as the SCR power is stepped from 10% power, to 50% power, and then back to 10% power.

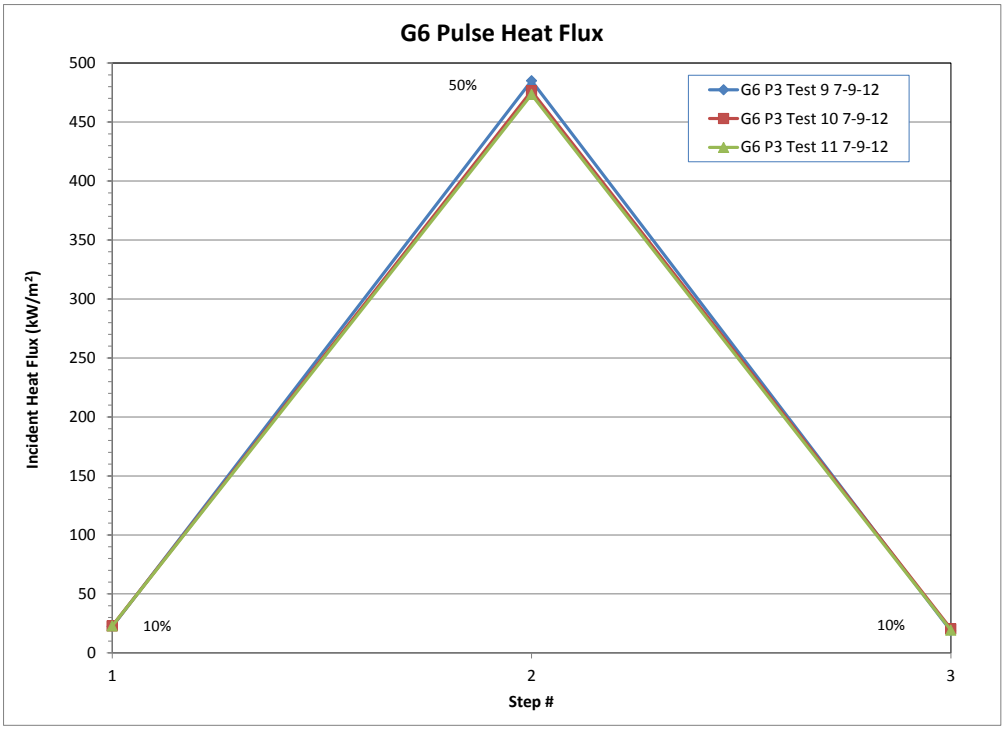

Figure 52 HTHFS Gage 6 Pulse Test Series Flux Comparison

Table 28 HTHFS Gage 6 Heat Flux Average Results - Three Pulse Tests

G6 SCR %	G6 Pulse flux average	1 std.dev.	power average	1 std.dev.
10	22.7	0.3	56.6	0.4
50	478.3	6.1	659.8	2.5
10	19.4	0.9	51.1	0.1

Table 29 provides the average power (kW) and standard deviation for all gages in all pulse tests, indicating very little difference between tests.

Table 29 Average and S.D. of SCR Power (all gages in all pulse tests)

SCR %	power average (all pulse tests)	1 std.dev.
10	57.7	1.0
50	669.1	7.5
10	52.0	0.6

9. SUMMARY

The average heat flux over the four second steady-state intervals for all gages in both the pulse tests and the step tests are compared in Figure 53 and Figure 54, respectively. Overall, at the highest flux level tested, agreement was within approximately 5 percent (Table 30) for the pulse tests and 22 percent (Table 31) for the step tests (10 percent for the step tests if only the first test for the HTHFS Gage 6 and Gage 6a are included). The HTHFS gages appear to be quite useful (once the reason for the variance between tests is understood) to measure flux to objects in abnormal thermal environments (e.g. sooty hydrocarbon fires) since they are small, unobtrusive, simple to use, have no windows that soot up, and require no water cooling.

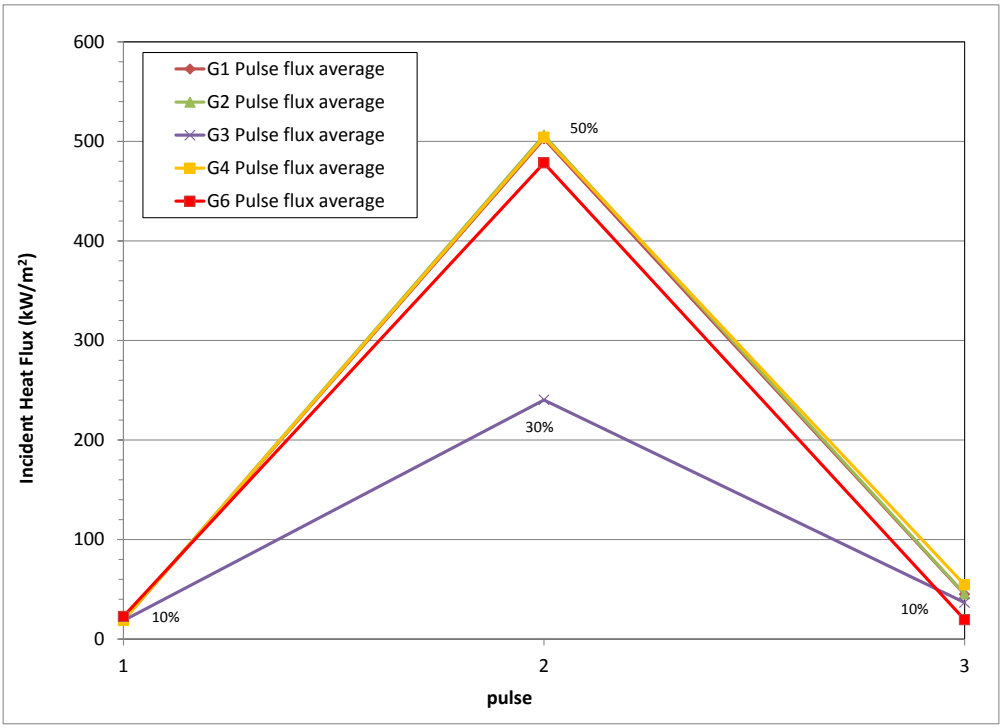

Figure 53 All Gages - Heat Flux Comparison - Pulse Tests

Table 30 All Gages - Average Flux for the 3 Pulse Tests

Gage/SCR Power	10%	50%	10%
1 Gardon	19.1	502.6	45.0
2 Schmidt-Boelter	19.0	506.1	45.4
3 Hukseflux	18.6		36.6
4 DFT	19.1	504.1	54.4
6 HTHFS	22.7	478.3	19.4
Max diff, kW/m^2	4.1	27.9	25.9
Max diff, %	21.9	5.8	133.6

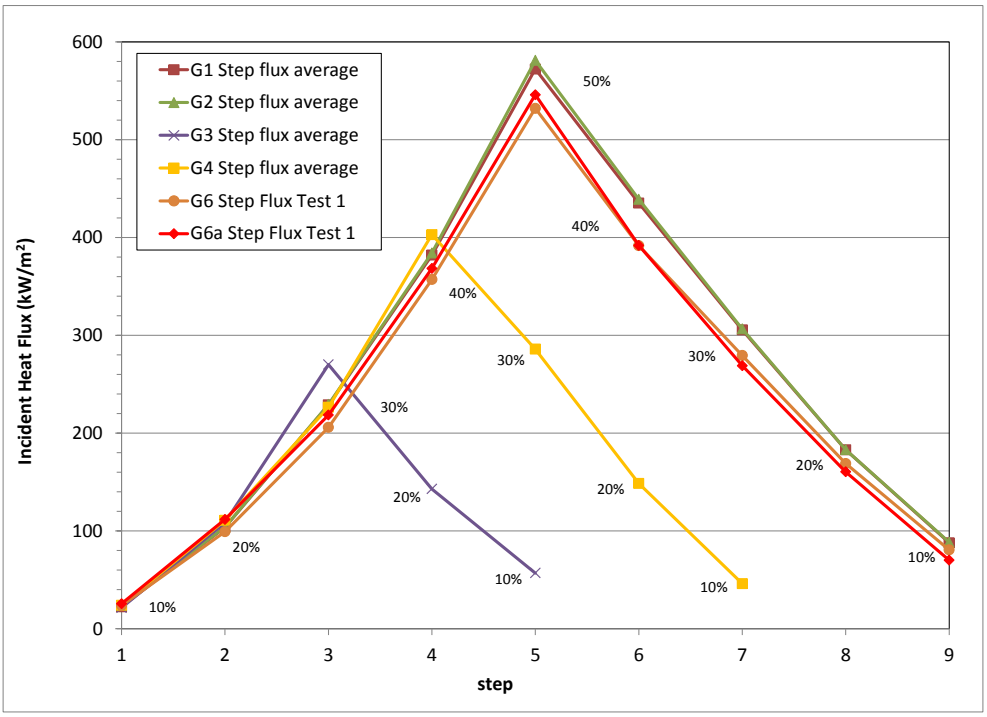

Figure 54 All Gages - Heat Flux Comparison - Step Tests

Table 31 All Gages – Average Flux for the 3 Step Tests

Gage/SCR Power	10%	20%	30%	40%	50%	40%	30%	20%	10%
1 Gardon	22.4	103.7	228.8	381.9	572.2	435.1	305.5	182.9	87.8
2 Schmidt-Boelter	23.9	103.9	229.3	384.1	581.0	438.9	306.5	183.0	88.4
3 Hukseflux	21.4	108.4	270.0					142.8	56.9
4 DFT	23.9	110.8	226.3	402.9			285.8	148.4	46.1
6 HTHFS	21.9	92.3	192.6	336.4	499.3	369.5	263.2	158.6	75.4
6a HTHFS	21.8	92.6	185.4	318.2	479.3	352.7	244.7	144.4	63.4
Max diff, kW/m^2	2.5	16.1	84.6	65.9	101.7	86.2	61.8	40.2	31.5
Max diff, %	11.7	17.5	45.6	20.7	21.2	24.4	25.2	28.1	55.4

10. REFERENCES

Beck, J. V., 1999, *"Users Manual for IHCP1D," a Program for Calculating Surface Heat Fluxes from Transient Temperatures Inside Solids,* Beck Engineering Consultants Co., Okemos, Michigan, 48864, October 30, 1999.

Blackwell, B. F., Douglass, R. W., and Wolf, H., 1980, "A Users Manual for the Sandia One-Dimensional Direct and Inverse Thermal (SODDIT) Code," Sandia National Laboratories report SAND85-2478, UC-32, Printed May 1987, Reprinted December 1980.

Blanchat, T. K., Humphries, L. L., and Gill, W., 2000, *"Sandia Heat Flux Gauge Thermal Response and Uncertainty Models,"* SAND2000-1111, Sandia National Laboratories, Albuquerque, NM, May 2000.

Figueroa, V. A., Nakos, J. T., and Murphy, J. E., 2005, *"Uncertainty Analysis of Heat Flux Measurements Estimated Using a One-Dimensional Inverse Heat Conduction Program,"* SAND2005-0039, Sandia National Laboratories, Albuquerque, NM, February 2005.

Gifford, A. R., et al., "*Durable Heat Flux Sensor for Extreme Temperature and Heat Flux Environments,"* Journal of Thermophysics and Heat Transfer, Vol. 24, No. 1, January-March 2010.

Hubble, D. O. and Diller, T. E., 2010, *"A Hybrid Method for Measuring Heat Flux,"* Journal of Heat Transfer, Vol. 132, March 2010.

Nakos, J. T., 2004, *"Uncertainty Analysis of Thermocouple Measurements used in Normal and Abnormal Thermal Environment Experiments at Sandia's Radiant Heat Facility and Lurance Canyon Burn Site,"* SAND2004-1023, Sandia National Laboratories, Albuquerque, NM, April 2004.

Nakos, J. T., 2005, *"Uncertainty Analysis of Steady State Incident Heat Flux Measurements in Hydrocarbon Fuel Fires,"* SAND2005-7144, Sandia National Laboratories, Albuquerque, NM, December 2005.

Pitts, W. et.al, 2004, *"Round Robin Study of Total Heat Flux Gage Calibration at Fire Laboratories,"* NIST Special Publication 1031, October 2004.

Raphael-Mabel, S. et.al., 2005, *"Design and Calibration of a Novel High Temperature Heat Flux Gage,"* HT-2005-72761, Proceedings of 2005 ASME Summer Heat Transfer Conference, San Francisco, CA, July 17-22, 2005.

APPENDIX A: DFT TEMPERATURE-DEPENDENT THERMAL PROPERTIES

Inconel (Thermal Properties of Structural Materials Found in Light Water Reactor Vessels, INL/EXT-09-16121

Temperature (C)	Density (kg/m3)	Specific Heat (J/kg-K)	Thermal Conductivity (W/m-K)
0	8736	450	9.8
20	8735	450	10.2
200	8700	454	13.4
300	8670	457	15.2
400	8635	465	17.0
500	8596	488	18.8
600	8553	536	20.6
700	8507	584	22.4
800	8457	605	24.2
900	8406	613	26.0
1000	8351	619	27.8
1100	8295	629	29.6
1200	8237	642	31.4
1300	8178	660	33.2
1400	8117	682	35.0

Cerablanket (Kaowool - 8PCF, nominal density 128 kg/m3)[1]

Temperature (C)	Specific Heat (J/kg-K)	Thermal Conductivity (W/m-K)
-53	810	0.029
20	855	0.035
22	856	0.035
24	858	0.035
27	859	0.036
30	861	0.036
144	927	0.049
243	980	0.062
333	1025	0.077
520	1107	0.115
543	1116	0.120
653	1157	0.148
760	1193	0.179
794	1203	0.189
928	1239	0.234
1059	1267	0.284

[1] Estimated Local Thermal Conductivity of 8PCF Cerablanket based on ASTM C201 test data (101503) - Courtesy of Roger Oxford at Thermal Ceramics and Ned Keltner of Sandia National Laboratories (retired).

APPENDIX B: VIRGINIA TECH HIGH TEMPERATURE HEAT FLUX SENSOR (HTHFS)

(Clay Pullins, cpullins@vt.edu, May 20, 2011)

The HTHFS is a conduction thermopile gage for which a temperature difference is measured across a known thermal resistance. Lead wire configuration permits simultaneous measurement of sensor surface temperatures (top and bottom) and heat flux*. The maximum operating temperature (long duration) of the HTHFS is 1000°C.

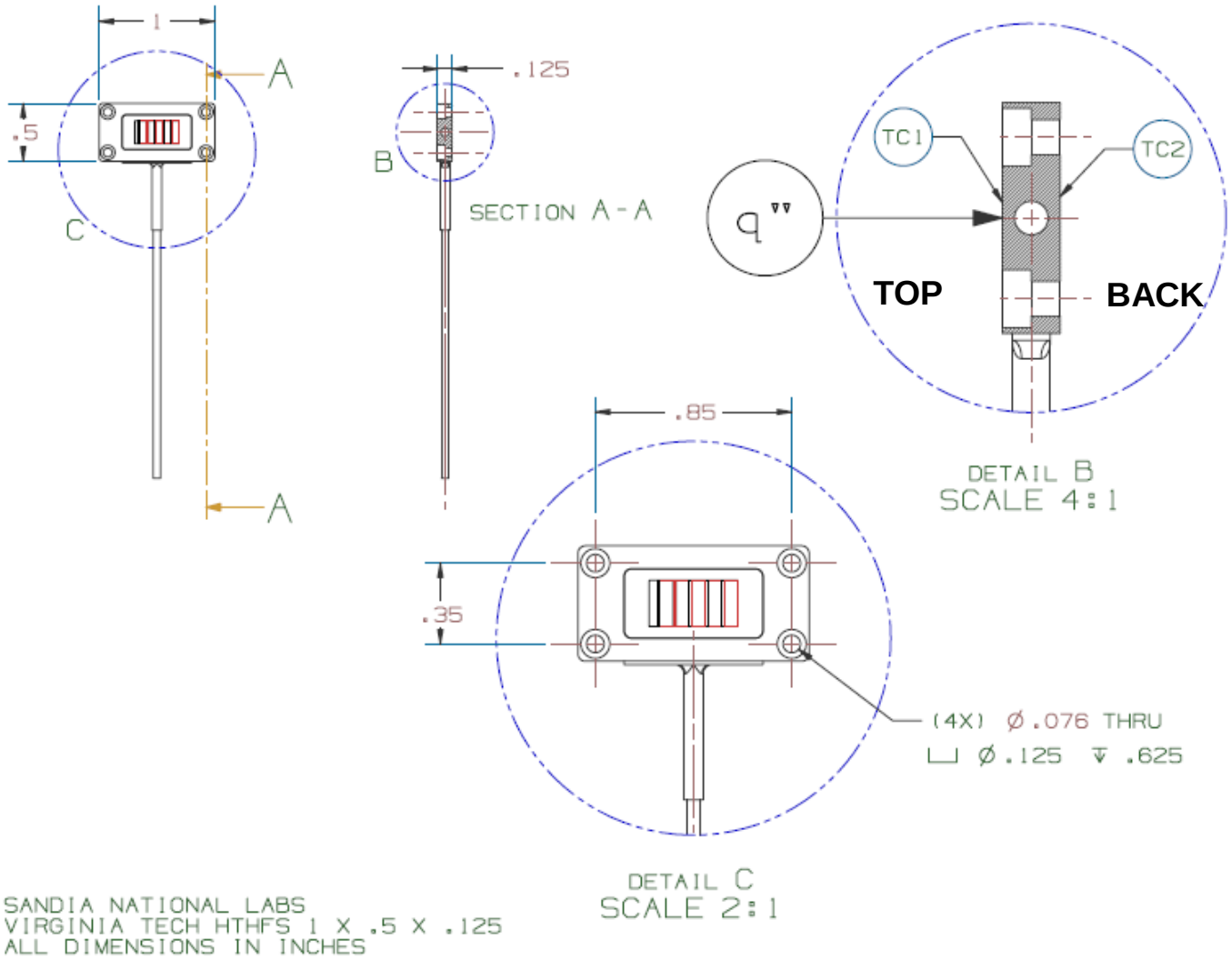

The two surface temperatures are measured by K-type thermocouples in the location as shown above. Each sensor has two male mini-plug thermocouple connectors (Omega part# SMPW-K-MF) labeled TC1 and TC2, corresponding to the measurement location depicted above. As convention, we say that TC1 measures the sensor's "TOP" temperature and TC2 measures the sensor's "BACK" temperature. Also, positive heat flux ($q''+$) is heat flowing INTO the TOP surface, as depicted above. The sensor measures heat flow in either direction, however this is just our convention for lead wire labeling / orientation.

Connection Diagram:

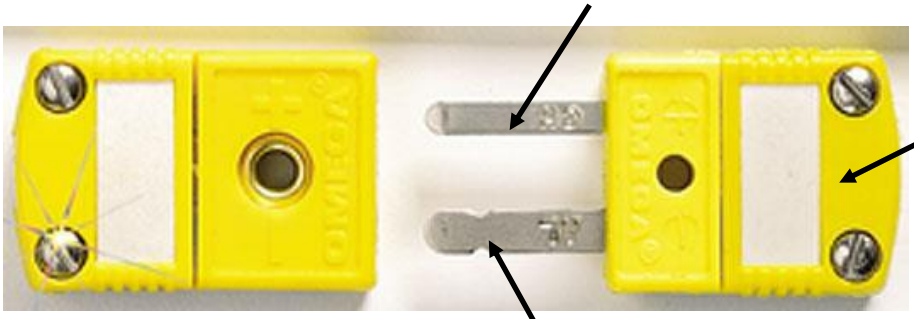

Omega part# SMPW-K-MF

Polarity Chart:

Measurement	**(+) Positive Terminal**	**(-) Negative Terminal**
TOP Surface Temperature	TC1 – Chromel Leg (+)	TC1 – Alumel Leg (-)
BOTTOM Surface Temperature	TC2 – Chromel Leg (+)	TC2 – Alumel Leg (-)
Heat Flux (Primary)	TC2 – Chromel Leg (+)	TC1 – Chromel Leg (+)
Heat Flux (Secondary)*	TC2 – Alumel Leg (+)	TC1 – Alumel Leg (+)

*The lead wire configuration allows the measurement of two heat flux voltages. The chromel-chromel (Cr-Cr) voltage is considered the primary voltage. The alumel-alumel (Al-Al) voltage is considered the secondary voltage. The Al-Al output is higher than the Cr-Cr output due to the addition on one thermocouple junction pair, however, the Al-Al output is more susceptible to two-dimensional heat transfer effects.

VT Room Temperature Calibration Results

Room temperature calibrations are performed using a halogen lamp bank facility. The incident radiation from the lamp bank is characterized with a water-cooled reference standard Schmidt-Boelter heat flux sensor, manufactured and calibrated by Medtherm Corporation. Each HTHFS is subjected to three levels of incident heat flux, while the sensor is maintained at room temperature (25°C). The sensitivities reported in the following table are for absorbed heat flux, $q''_{net} = \alpha q''_{incident}$. The surface absorptivity is $\alpha = 0.9$.

Sensor #	**Chromel-Chromel Sensitivity S_1 (25°C) (μV/W/cm^2)**	**Alumel-Alumel Sensitivity S_2 (25°C) (μV/W/cm^2)**
1	437.3	540.8
2	403.8	551.9
3	427.2	563.5

VT High Temperature Radiation Calibration Results:

High temperature radiation calibration was performed to assess the output temperature dependence of the HTHFS. The following plot shows the HTHFS sensitivity as a function of average sensor temperature. The y-axis represents the ratio of HTHFS sensitivity (at temperature) to the sensitivity at room temperature, and the x-axis represents the sensor's average temperature. The HTHFS output temperature dependence was calibrated up to 900°C.

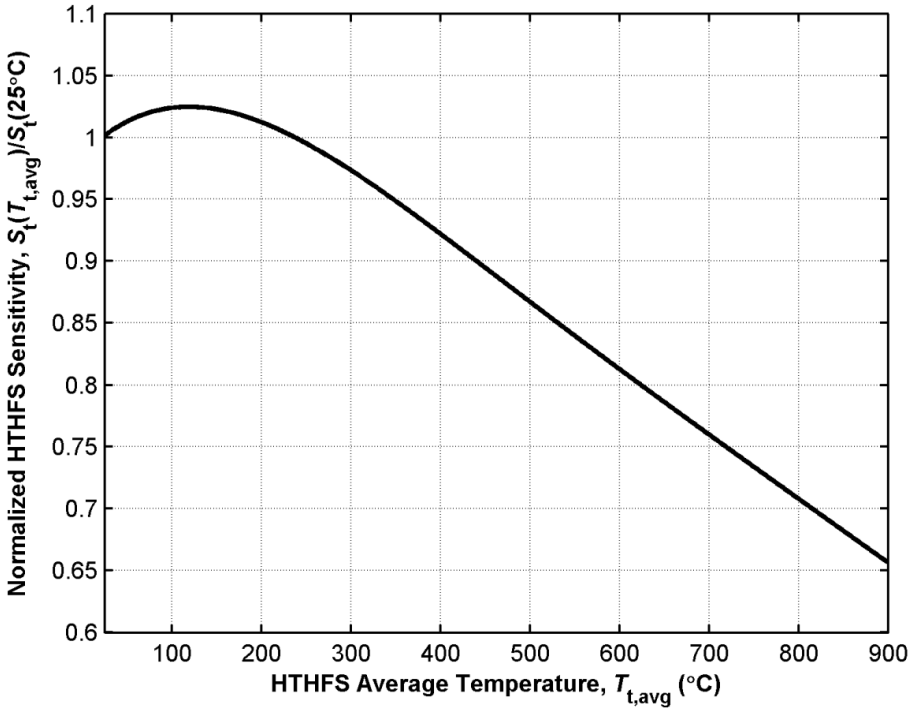

5th Order Polynomial Function, *T* in °C from 25 - 900 °C:

$$q'' = \frac{V_{out}}{S(T)} \quad ; \quad S(T) = S(25℃) \times (AT^5 + BT^4 + CT^3 + DT^2 + ET + F)$$

Polynomial Coefficients:

A =	1.2846e-015
B =	-4.5081e-012
C =	6.1663e-009
D =	-4.0540e-006
E =	7.3190e-004
F =	1.0

Thermal Mass Measurement of HTHFS

To measure the per area thermal mass (***ρCδ***, product of density, specific heat, and thickness) of the HTHFS, it was insulated and positioned in front of the calibrated halogen lamp in order to subject it to a known incident radiation. Each sensor was subjected to four different heat fluxes between approximately 1.5 and 6.5 W/cm^2. A shutter was used to subject the sensor to a step change in heat flux. During the test, the thermocouples built into the HTHFS were used to measure the temperature history of the top and bottom of the sensor. Assuming that no heat leaves the backside of the HTHFS, all the heat that enters the sensor is stored by the sensor.

$$q'' = \rho C \delta \frac{dT_{ave}}{dt} \tag{1}$$

The average sensor temperature is taken as the arithmetic mean of the two sensor temperature measurements. The figure below is a plot of the measured average temperature history for four tests divided by the constant applied heat flux for that test (***T_{ave}/q''*).** The linearity of the collapse is an indication that the assumption of no heat conduction out the back of the sensor is valid. The value of ***ρCδ*** is then calculated from the inverse of the slope of the curve in the following figure:

$$\frac{1}{\rho C \delta} = \frac{d}{dt}\left(\frac{T}{q''}\right) \tag{2}$$

The measured per area thermal mass values are given in the following table:

Per area thermal mass measurements:

Sensor #	***ρCδ*** (J/(cm^{2}K)
1	**1.30**
2	**1.29**
3	**1.28**

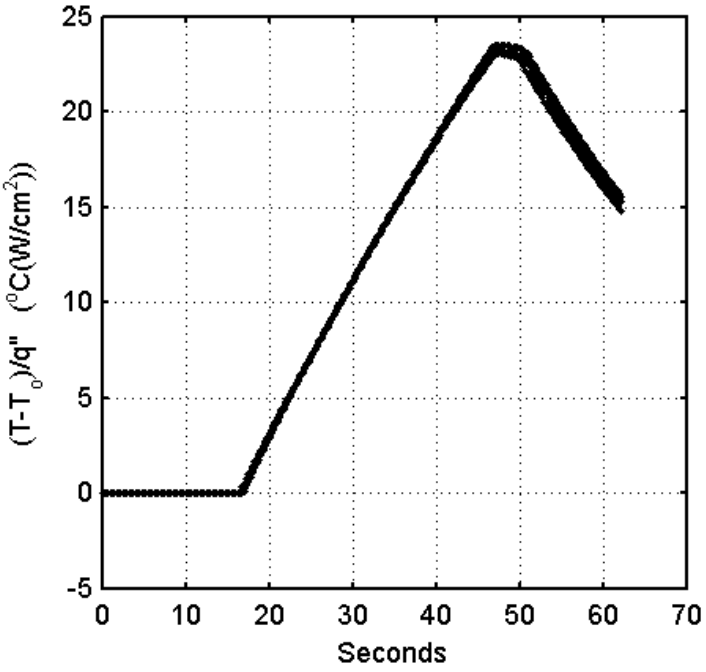

Average sensor temperature history divided by applied heat flux

DISTRIBUTION

1 Virginia Polytechnic Institute and State University
Mechanical Engineering Dept.
Attn: Thomas E. Diller
Blacksburg, VA 24061-0238

1	MS1135	Thomas Blanchat	1532
1	MS1135	Chuck Hanks	1532
1	MS1135	Pat Brady	1532
1	MS1135	Sylvia Gomez	1532
1	MS1135	Dann Jernigan	1532
1	MS1135	Shane Adee	1532
1	MS1135	Jerry Koenig	1532
1	MS1135	Brandon Servantes	1532
1	MS1135	Jill Suo-Anttila	1532
1	MS1135	Alex Brown	1532
1	MS1135	Allen Ricks	1532
1	MS1135	Randy Watkins	1532
1	MS0386	Jim Nakos	2129
1	MS0899	Technical Library	9536 (electronic copy)


Sandia National Laboratories